

A POLARIZATION SURVEY OF SiO MASER VARIABILITY IN EVOLVED STARS

J. Glenn¹, P.R. Jewell², R. Furre¹, and L. Miaja¹

ABSTRACT

We have monitored the SiO ($v = 1, J = 2 \rightarrow 1$) maser polarization in 17 variable stars (Miras, OH-IR stars, and supergiants) to investigate the long-term persistence of masers. The 8 epochs of observations span 2.5 years, thereby sampling multiple cycles for these stars with typical periods of ~ 1 year. The average polarization was 23% with a typical dispersion of 7%, although the variability differed substantially from star to star. In the Stokes q and u spectra of individual stars, a few strong maser features tended to dominate the polarization, with the maser features persisting for less than one stellar cycle for some stars, and for multiple cycles for a few stars. Because individual masers are not resolved in our beam-averaged total intensity spectra, we correlated the polarization spectra between epochs to measure the characteristic lifetimes of the features, rather than attempting to trace the evolution of separate line components. We found that individual maser feature lifetimes ranged from a few months or less to > 2 years. These data indicate that for the sample of stars as a whole, the masers are not reset at a particular stellar phase.

Subject headings: masers, silicon monoxide, polarization, stellar atmospheres, stars: red giants, miras, OH-IR stars

1. Introduction

SiO masers are found in a variety of evolved giant and super-giant stars, including Miras, semi-regular variables, M super-giants, and OH/IR stars. Giant and supergiant stellar atmospheres and their mass loss mechanisms are not fully understood: convection and composition variations are complex, and detailed atmospheric models are just emerging. The

¹CASA, University of Colorado, 389-UCB Boulder, CO 80309, USA

²National Radio Astronomy Observatory, P.O. Box 2, Green Bank, WV 24944. The National Radio Astronomy Observatory is a facility of the National Science Foundation operated under cooperative agreement by Associated Universities, Inc.

location of SiO masers, close to the photospheres, makes them useful probes of the extended atmospheres and the mass loss phenomenon.

Spectroscopy of evolved stars has shown significant variability in maser intensities and line widths (Clark, Troland, & Johnson 1982; Clark et al. 1984; Barvainis & Predmore 1985; Jewell et al. 1991; Herpin et al. 1998). ^{28}SiO (hereafter simply SiO) masers have been observed in rotational transitions from $J = 1 \rightarrow 0$ to $J = 7 \rightarrow 6$ and from vibrational states $v = 0$ to $v = 3$, from frequencies of 43 GHz to 302 GHz (Jewell et al. 1987; Pijpers, Pardo, & Bujarrabal 1994; Cho, Kaifu, & Ukita 1996; Gray et al. 1997). VLBI observations have revealed that the masers are generally located in ring structures in the circumstellar envelopes (Diamond et al. 1994; Miyoshi et al. 1994; Greenhill et al. 1995; Humphreys et al. 1996; Colomer et al. 1996; Boboltz, Diamond, & Kemball 1997; Doeleman, Lonsdale, & Greenhill 1998). Ring radii typically range from 1.5 to 4 stellar radii. Since the observed rings present themselves perpendicular to the line of sight, it has been postulated that the masing takes place on the surfaces of spheres centered on the stars, and that the masing radiation escapes tangentially to the spheres. Combined with the tangential polarization vectors, this structure has been taken as evidence for radiative pumping of the masers (Desmurs et al. 2000).

Previous observations of some Miras indicated that individual maser spectral features appeared to persist throughout entire stellar cycles (e.g., Clark et al. 1984). However, the continuity of maser features was also found to be disrupted at various times throughout the stellar cycles, including at maximum light (e.g., Clark, Troland, & Miller 1985) and at SiO maser brightness minimum (Martínez, Bujarrabal, & Alcolea 1998). It has been proposed that the masers are created anew by periodic shock waves propagating through the extended atmospheres and lagging the optical maximum by about ~ 0.2 periods (Clark et al. 1984). Recent numerical models have been used to simulate the SiO maser variability with a constant infrared radiation field combined with shocks (Humphreys et al. 2002).

To investigate the relationship between maser variability and stellar cycle, we observed the 86.2434 GHz SiO ($v = 1$, $J = 2 \rightarrow 1$; antenna temperature and polarization) transition in 17 evolved stars during eight epochs over two and a half years. Our observations are not densely sampled enough to investigate the detailed evolution of masers in any star within a stellar cycle. However, the large survey size, with sampling up to four stellar cycles per star, enables us to quantify the long-term polarization behavior of the masers, complementary to detailed studies of individual stars. §2 describes our observations and §3 presents the results and discussion. Our conclusions are summarized in §4.

2. Observations

The observations were made with the facility polarimeter and 3-mm receivers at the NRAO 12 Meter Telescope on Kitt Peak in standard position-switching mode. A parallel-wire grid and mirror combination, with a tuned separation acting as a half-waveplate, modulated the polarization. The waveplate was stepped to 16 positions per rotation, allowing for four independent measurements of polarization per rotation. Systematic, instrumental polarization was measured with observations of planets, and found to be small ($\ll 1\%$) compared to the observed stellar polarizations. The orthogonal senses of polarization were split by another parallel-wire grid and transmitted to two receivers. The polarization efficiency and position angle were calibrated with a linearly-polarized noise source mounted at the center of the subreflector. The parallactic angle correction was verified with observations of the Crab Nebula. We used two 128-channel filter bank backends for each receiver, with 100 kHz and 250 kHz resolutions, corresponding to 348 and 870 m s^{-1} , respectively. The 250 kHz spectra were used only to cross-check the 100 kHz spectra. Each star was observed one or more times per day, weather permitting, during the following eight epochs: 1995 April, 1995 October, 1996 March, 1996 July, 1996 September, 1997 February, 1997 June, and 1997 October. Calibration was done on the T_R^* scale. The conversion factor to flux density is 32 Jy/K(T_R^*). The stellar phases and periods were derived from Kholopov (2002) and the AAVSO data base (<http://www.aavso.org/adata/onlinedata/>). Throughout this paper, the stellar phases are referred to the optical maxima. The spectra and polarizations for each star for each epoch are displayed in Figures 8 to 24..

3. Data Analysis and Discussion

3.1. Periodicity of SiO Brightness

The peak line temperatures vary dramatically, up to nearly a factor of 100 for R Hya from stellar phase 0.15 to 0.97. Previous observations have revealed periodic maser line temperature variations matched to the stellar periods but with a phase lag of ~ 0.2 periods (Clark et al. 1984; Gray et al. 1997). To test for this signal in our data, for each star we summed the antenna temperatures in each backend channel over the entire spectral line, normalized the sums to the maximum observed line temperature, and plotted them versus the stellar phase (Figure 1). For the ensemble, the integrated line temperatures are clearly periodic. A least-squares best-fit sine wave fits the aggregate-normalized maser temperatures well with a phase lag of $\Delta\phi = 0.11$ and an uncertainty $\sigma_{\Delta\phi} = 0.03$, in broad agreement with the previous results, but tending toward a slightly smaller phase shift.

3.2. General Characteristics of Maser Polarizations

The Stokes parameters were calculated for each velocity channel for each observation (Figures 8 through 25): I , q (N-S polarized T_R^* minus E-W polarized T_R^*), and u (NE-SW polarized T_R^* minus NW-SE polarized T_R^*), with polarization $P = \sqrt{q^2 + u^2}/I$ and position angle $\theta = \frac{1}{2}\tan^{-1}(\frac{U}{Q})$, where $Q = q/I$ and $U = u/I$ are the normalized Stokes parameters and $I = T_R^*$. Since we are interested in the long term variability, we averaged the Stokes spectra for each star for the multiple observations at each epoch (separated by no more than a couple of days).

The spectra are complex with several line components visible in most of them. In general, the polarizations are dominated by a few highly-polarized components that can be distinguished by their q 's and u 's. Since our observations beam-average all the masers within each stellar envelope, it is possible that multiple masers contribute to each observed feature at a given velocity. Overlapping features could explain the smooth variations in polarization and position angle (given by changing relative contributions from q and u) across the spectra. For example, R Aqr is dominated by 1-3 components that tend to blend together for all the epochs in our survey. In contrast, *o* Ceti, VY CMa, U Her, R Leo, and VX Sgr have separate line components that can be distinguished even in the absence of polarization information. Under the assumption that the masing cells are distributed in a ring-like manner with tangential polarization vectors, the line blending of multiple components will reduce the observed polarization. Thus, our interpretation of independent masers leads to a lower limit to the actual polarization of independent masing entities.

As a broad characterization of the maser polarization, we averaged the polarization across the spectral lines for each star for each epoch. The percentage polarizations are shown as a function of Julian Day in Figure 2. The spectrum-averaged polarization varies substantially for most of the stars. However, stars with high average polarization tended to retain a high polarization: *o* Ceti ($\langle P \rangle = 44\%$, rms = 9%) and S CrB ($\langle P \rangle = 41\%$, rms = 8%). Stars with moderate polarization tended to retain moderate polarization, and stars with low polarization tended to retain low polarization, e.g., VX Sgr ($\langle P \rangle = 5\%$, rms = 2%; see Figure 3, where $\sigma_P/\langle P \rangle < 1$ for all of the stars). The average polarization for all the stars over all the epochs was 23% (Table 1).

To look for evidence of cyclic polarization variation, the polarization is plotted in Figure 4 versus the stellar phase ϕ . No significant systematic polarization variability is apparent, with the possible exception of a minimum at $\phi = 0.2$, approximately corresponding to the peak in maser brightness. This minimum at $\phi = 0.2$ is suspect: a single observation of 40% polarization at $\phi = 0.2$ would make the apparent minimum invisible. The most highly polarized star, *o* Ceti was not observed near $\phi = 0.2$, and if it had been the visual impression

of a minimum likely would be absent.

A subtle shift in polarization as a function of stellar phase can be tested by binning the polarizations for the ensemble into the high intensity phase (corresponding to the brightest half of each cycle for SiO; $0.85 < \phi < 0.35$ in Figures 1 and 4) and the low intensity phase ($0.35 < \phi < 0.85$). Excluding VY CMa, which is aperiodic, and OH2.6-0.4, for which we did not find a single stellar maximum, the average high intensity phase polarization was 23% ($\sigma = 4\%$; standard deviation of the mean) and the average low intensity phase polarization was 23% ($\sigma = 3\%$; standard deviation of the mean). Thus there is no convincing evidence of systematic polarization variability in the high intensity phase compared to the low intensity phase.

The integrated line temperatures were higher during the high intensity phase than during the low intensity phase by an average factor of 1.3. Under the assumption that the masers are distributed on circumstellar rings with tangential polarization vectors, we can relate the integrated line temperatures and percentage polarizations. An increased number of masers with a constant average brightness (leading to the increased high intensity phase brightness) would tend to decrease the beam-averaged polarizations by a factor of \sqrt{n} (in the limit of large n), where n is the number of independent masers. For a brightness increase of 1.3, the polarization would be expected to fall by a factor of 1.14 from 23%, during the low intensity phase, to 20% during the high intensity phase (for $n \propto T_R^*$). Since the percentage polarization is actually equal during both phases at 23% and the 1σ uncertainty in the difference is 5%, the interpretation is inconclusive. The spectra themselves do not show a clear dependence on the number of line polarization features as a function of stellar phase, although polarization spectral features should not be assigned to discrete masers due to the beam averaging.

The spectrum-averaged polarization position angles θ do not have random distributions for many of the stars in our sample (Figure 5). This either indicates: 1) that there is some long-term ($\Delta\phi > 1$) persistence in the masers, or 2) if the masers are distributed in circumstellar rings with tangential polarization vectors, that particular regions in the circumstellar envelopes tend to consistently mase most brightly for $\Delta\phi > 1$, or both. R Aqr, VY CMa, *o* Ceti, and S CrB, for example, have position angles that slowly vary around mean values, with position angle dispersions σ_θ of 30° , 5° , 20° , and 19° , respectively. VY CMa is dominated by just a few small features that remain coherent for the entire span of our observations. So, for these stars, even if the discrete masers do not remain coherent for greater than one period, the masing is dominated by one or two (opposing) quadrants of the stellar disks. However, this is not true for all the stars: the mean $\sigma_\theta = 49^\circ$, indicating that dominant maser coherence is not maintained for $\Delta\phi > 1$ in general.

3.3. Estimation of Maser Lifetimes

To quantitatively test the prediction that masers are reborn each stellar cycle with the passage of a shock wave, we compared the polarization spectral feature lifetimes, which are assumed to be representative of the maser lifetimes, with the stellar periods. To avoid the ambiguities associated with the decomposition of a continuous spectrum into a discrete sum of spectral components, we used a statistical method to estimate the feature lifetimes. In addition to numerical simplicity, this approach takes in account all maser polarization, even from features too small to be individually extracted. Although all maser emission in the spectra contribute to the derived lifetimes, brighter components contribute more than fainter ones. This technique does not require assigning individual masers to spectral polarization features on a one-to-one basis.

For computational convenience, each spectrum was treated as a complex function $S(\nu)$ of velocity, where $q(\nu)$ was the real part and $u(\nu)$ was the imaginary part (similarly, the polarization could be represented in polar coordinates: $P = P_0 e^{i\theta}$). We write the correlation C_{ij} between the spectra of two epochs i and j , observed at times T_i and T_j , as

$$C_{ij} = \frac{\int_{\nu_L}^{\nu_U} S_i(\nu) \cdot S_j(\nu) d\nu}{\left[\int_{\nu_L}^{\nu_U} |S_i(\nu)|^2 d\nu \int_{\nu_L}^{\nu_U} |S_j(\nu)|^2 d\nu \right]^{1/2}}. \quad (1)$$

The time between the two observations i and j is $\Delta T_{ij} = T_j - T_i$, and the integrals are numerical sums over the spectral lines binned in velocity by the receiver backends. C_{ij} would be unity for $i = j$, and one expects the C_{ij} 's to become smaller as ΔT_{ij} increases and the masers evolve, come, and go. To estimate an average maser lifetime for a star, the width of $(\Delta T_{ij}, C_{ij})$ distribution for all ij pairs was fit to a gaussian expectation function $H(\Delta T)$ with width (in time) given by σ . With this formalism, the width in the correlation function is $\sqrt{2}\sigma$, and we take the average spectral feature lifetime to be 2σ . The average spectral component lifetime is not the lifetime of a maser, but represents a characteristic time over which the q and u spectral features persist.

The stars were sampled from one to six times per period (typically 2-3 times per period), with an average of 6.4 observations per star over 30 months, and a typical time between observations of 3.75 months. Therefore, lifetimes shorter than a few months or greater than 30 months cannot be measured. The uncertainties in the fits of the correlation distribution to the expectation function were on the order of 1-2 weeks, but the systematic errors in applying this technique to poorly sampled data should dominate the uncertainties.

Average maser lifetimes derived with this technique range from 85 to 800 days, with the

lowest number corresponding well to the minimum time between observations. The lifetimes are plotted versus the stellar periods in Figure 6; the stellar periods cluster at just over one year. Long lifetimes were derived for *o* Ceti (545 days) and S CrB (500 days). Inspection of their spectra in Figures 12 and 14, respectively, reveals several strong polarization features that persist for many of the observations, even for > 1 stellar period. R Leo, with a derived lifetime of 415 days, also exhibits the persistence of some features, enabling a robust lifetime to be derived. VY CMa is aperiodic, and hence does not appear in Figure 6, but does have weak polarization features at ~ 0 km/s that persisted from 1996 March to 1997 October, and one feature at ~ -1.5 km/s that is present in all the epochs, consistent with the 645 day derived lifetime. For the majority of the stars in the sample, the characteristic lifetimes are shorter than the stellar periods, indicating that many masers do not survive entire stellar cycles. The OH-IR stars and supergiants do not seem to differ from the Miras in their maser lifetimes.

To summarize, one rule does not apply to all of the stars: some exhibit maser line features that persist for more than one stellar cycle, while others exhibit masers that do not persist for even a single full cycle. Beyond this, our survey does not have sufficient temporal resolution to determine whether most masers go through a “reset” at any particular phase.

3.4. Maser Line Widths

In a manner similar to the maser lifetime estimation, the maser line widths can be estimated in km/s without resorting to fitting multiple line components, which are not well constrained for low-level spectral features. We derived polarization line feature widths from the autocorrelation function $A(\Delta\nu)$ of the polarization spectrum $S(\nu)$:

$$A(\Delta\nu) = \int_{\nu_L}^{\nu_U} S(\nu)S(\nu + \Delta\nu)d\nu. \quad (2)$$

The $A(\Delta\nu)$ closely approximate Gaussians: in the limit that the spectrum $S(\nu)$ were the sum of Gaussian features of width σ , the autocorrelation function would be a Gaussian of width $\sqrt{2}\sigma$. We defined the average velocity dispersion as the dispersion that would produce an autocorrelation function best fitting the observed result $A(\Delta\nu)$.

Averaged over the ensemble, the velocity dispersion is 0.52 km s^{-1} . The range of widths is small, 0.33 to 0.67 km s^{-1} , suggesting that a common physical process leads to an upper limit for the maser velocity-widths, or that blending occurs on this scale due to beam averaging. Figure 7 shows that the maser feature line widths are independent of stellar phase, indicating that coherent masers are not velocity broadened by the stellar winds or pulsations during the stellar cycles.

4. Conclusions

We monitored the intensity and polarization of SiO masers in 17 evolved stars, over 2.5 years, to investigate the relationship between maser variability and stellar phase. The polarization variability is not uniform throughout the sample. Sustained polarizations of nearly 50% were observed in *o* Ceti, whereas a sustained polarization of $\sim 5\%$ was observed in VX Sgr, and the sample-average polarization was 23% with a typical dispersion of 7%. For the ensemble of stars, the polarization is not related to stellar phase, with the possible exception of a slight minimum in polarization at $\phi \sim 0.2$.

In the Stokes q and u spectra of individual stars, a few strong maser features tended to dominate the polarization. In some cases, these masers persisted for several epochs (> 1 stellar cycle), and in other cases they evolved much more quickly, with little resemblance between the spectra from subsequent epochs. We used a statistical technique to quantify the lifetimes of maser line polarization features (which may not correspond to independent masers in our beam-averaged observations) for comparison to the stellar periods. For each star, we measured the correlation between the spectra in all pairs of epochs as a function of the time between the epochs. This technique has the advantage of incorporating all of the polarization information in the spectra, without having to fit individual line components and trace them from epoch-to-epoch. For regular variable stars, we found that the characteristic maser lifetimes ranged from a few months (the minimum lifetime that could be measured) to 800 days. These data indicate that the masers are not reset by the passage of shocks every stellar cycle from stellar pulsations for some of the stars, and that the maser lifetimes are often shorter than the stellar periods for others.

We also found a long-term persistence in the spectrum-averaged polarization position angles for some of the stars. This is in broad agreement with the persistence of individual masers, or a preference for masing in single or opposing quadrants of the stellar disks (assuming ring-like distributions of masers with tangential polarizations). Finally, the widths of the maser line components in the spectra ranged from $\sim 0.3 - 0.7$ km/s, with no dependence on stellar phase.

5. Acknowledgments

We thank the AAVSO International Database and its observers worldwide for the dates of stellar maxima. We thank Phil Maloney for helpful discussions and Chris Walker for contributions to the design of the polarimeter.

REFERENCES

- Barvainis, R., & Predmore, C.R. 1985, ApJ, 288, 694
- Boboltz, D.A., Diamond, P.J. and Kemball, A.J. 1997, ApJ, 487, L147
- Cho, S-H., Kaifu, N. and Ukita, N. 1996, AJ, 111, 1987
- Clark, F.O., Troland, T.H. and Johnson, D.R. 1982, ApJ, 261, 569
- Clark, F.O., Pepper, G.H., Troland, T.H. and Johnson, D.R. 1984, ApJ, 276, 572
- Clark, F.O., Troland, T.H., & Miller, J.S. 1985, ApJ, 289, 756
- Colomer, F., Baudry, A., Graham, D.A., Booth, R.S., de Vincente, P., Krichbaum, T.P., Gómez-González, J., and Schalinski, C. 1996, A&A, 312, 950
- Desmurs, J.F., Bujarrabal, V., Colomer, F., & Alcolea, J. 2002, A&A, 360, 189
- Diamond, P.J., Kendall, A.J. et al. 1994, ApJ, 430, L61
- Doeleman, S.S., Lonsdale, C.J. and Greenhill, L.J. 1998, ApJ, 494, 400
- Gray, M.D., Ivison, R.J., Humphreys, E.M.L. and Yates, J.A. 1997, MNRAS, 295, 970
- Greenhill, L.J., Colomer, F., Moran, J.M., Backer, D.C., Damchi, W.C. and Bester, M. 1995, ApJ, 449, 365
- Herpin, F., Baudry, A., Alcolea, J. and Cernicharo, J. 1998, A&A, 334, 1037
- Humphreys, E.M.L., Gray, M.D., Yates, J.A., Field, D., Bowen, G. and Diamond, P.J. 1996, MNRAS, 282, 1359
- Humphreys, E.M.L., Gray, M.D., Yates, J.A., Field, D., Bowen, G.H., & Diamond, P.J. 2002, A&A, 386, 256
- Jewell, P.R., Dickinson, D.F., Snyder, L.E., & Clemens, D.P. 1987 ApJ, 323, 749
- Jewell, P., Snyder, L.E., Walmsley, C.M., Wilson, T.L. and Gensheimer, P.D. 1991, A&A, 242, 211
- Kholopov. 2002, “The Combined Table of General Catalogue of Variable Stars, Volumes I-IV, available from the Sternber Institute at <ftp://ftp.sai.msu.su/pub/groups/cluster/gcvs/gcvsiiii/>.

Martínez, A., Bujarrabal, V., & Alcolea, J. 1988, A&AS, 74, 273

Miyoshi, M., Matsumoto, K., Kamenno, S., Takaba, H. and Iwata, T. 1994, Nature, Vol 371,
395

Pijpers, F.P., Pardo, J.R. and Bujarrabal, V. 1994, A&A, 286, 501

Table 1.

Star	Stellar Type	Period (Days)	$\langle P(\%) \rangle$	$\sigma_P(\%)$	$\langle \theta(^{\circ}) \rangle$	$\sigma_{\theta(^{\circ})}$	Characteristic Maser Lifetime (Days)
R Aqr	Mira/symbiotic	387	18.7	5.2	-41	30	210
RX Boo	Mira	340	34.3	16.5	51	39	105
TX Cam	Mira	557	14.0	2.5	0	70	360
R Cas	Mira	430	23.2	8.5	15	69	260
<i>o</i> Cet	Mira	332	44.3	9.4	0	20	545
VY CMa	Supergiant	...	4.5	0.5	43	5	645
S CrB	Mira	360	40.7	8.1	55	19	500
χ Cyg	Mira	408	17.4	8.3	34	42	160
RU Her	Mira	485	24.0	7.0	7	47	85
U Her	Mira	406	17.7	3.0	7	59	310
R Hya	Mira	389	32.0	17.5	9	71	160
W Hya	Mira	361	16.6	7.9	35	27	125
R Leo	Mira	310	22.9	4.7	-19	65	415
VX Sgr	Supergiant	732	5.3	2.1	11	78	235
IK Tau	OH-IR	470	12.0	4.5	22	60	315
IRC+10011	OH-IR	660	15.3	5.3	35	45	160
OH2.6-0.4	OH-IR	...	27.2	4.3	-1	86	800

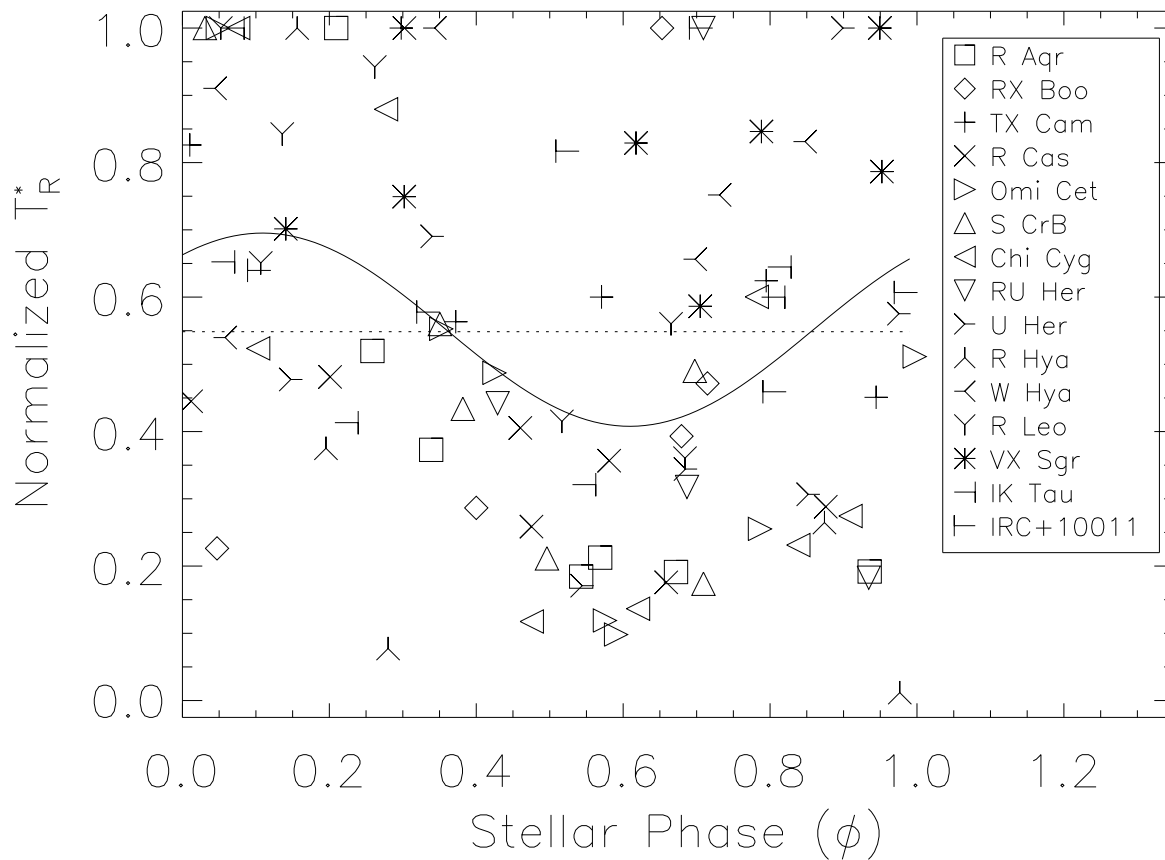


Fig. 1.— SiO line temperatures for the survey stars as a function of stellar phase. To facilitate comparison between the stars, the line temperatures, T_R^* , have been normalized for each star to the maximum observed line temperature for all of the epochs. The dotted line shows the mean for the ensemble, and the solid curve is the best-fit sine wave. The peak SiO brightness for the average is at a phase of 0.11, lagging the peak optical brightness.

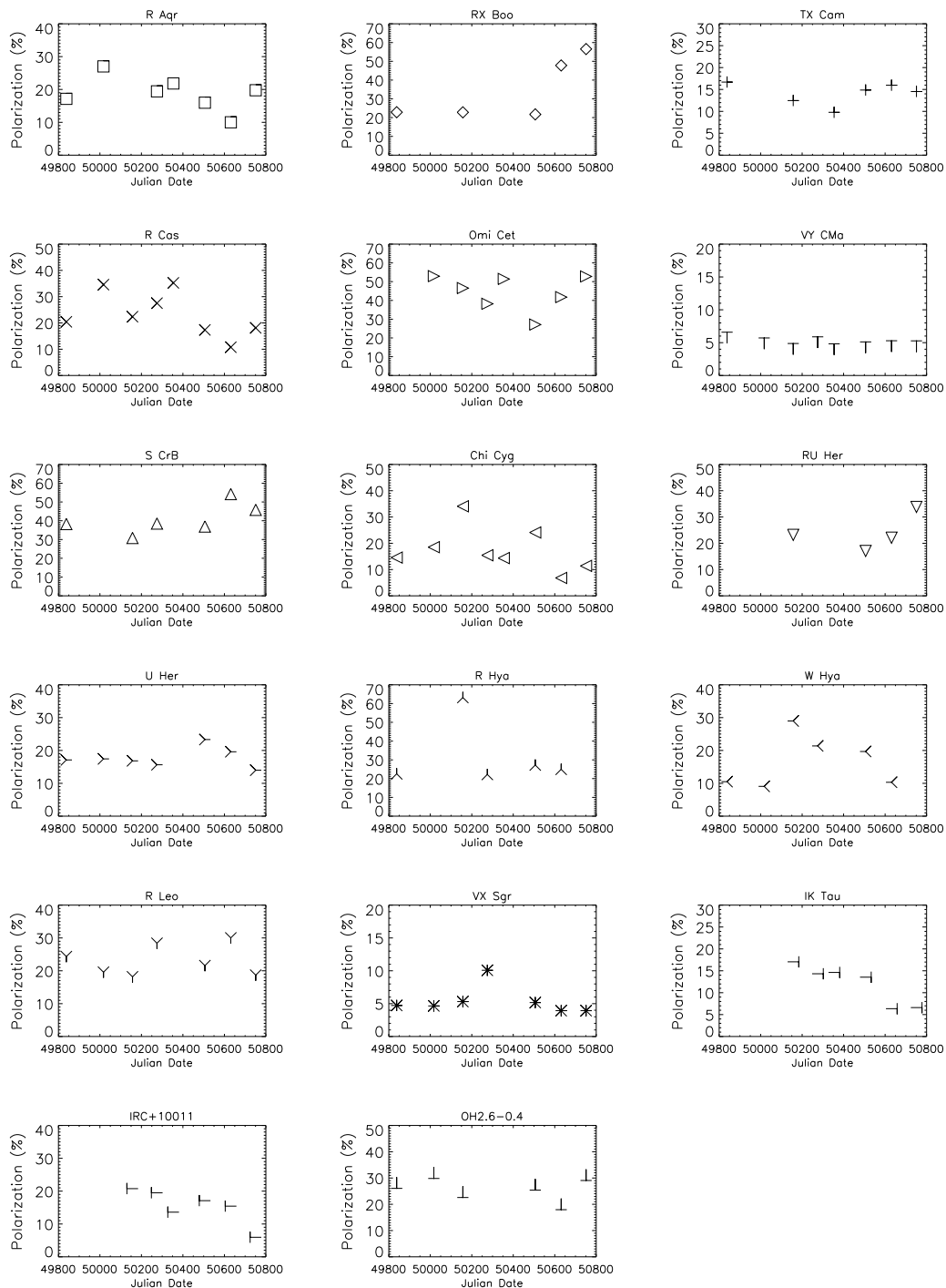


Fig. 2.— Line-integrated percentage polarization as a function of Julian Date. The full Julian Date for the first epoch of observations is 2449838. The highest polarization for R Hya has very low S/N, which leads to an erroneously high polarization.

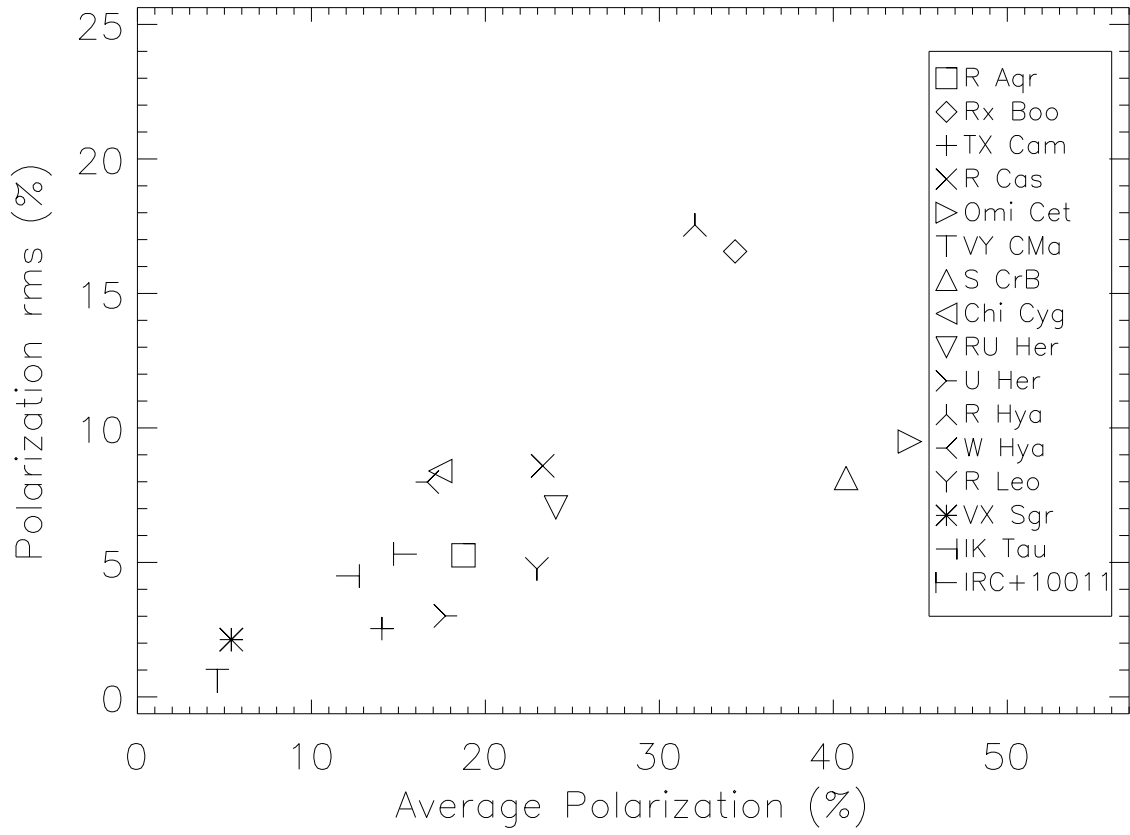


Fig. 3.— Line-integrated epoch-to-epoch polarization rms versus percentage polarization averaged over all the epochs.

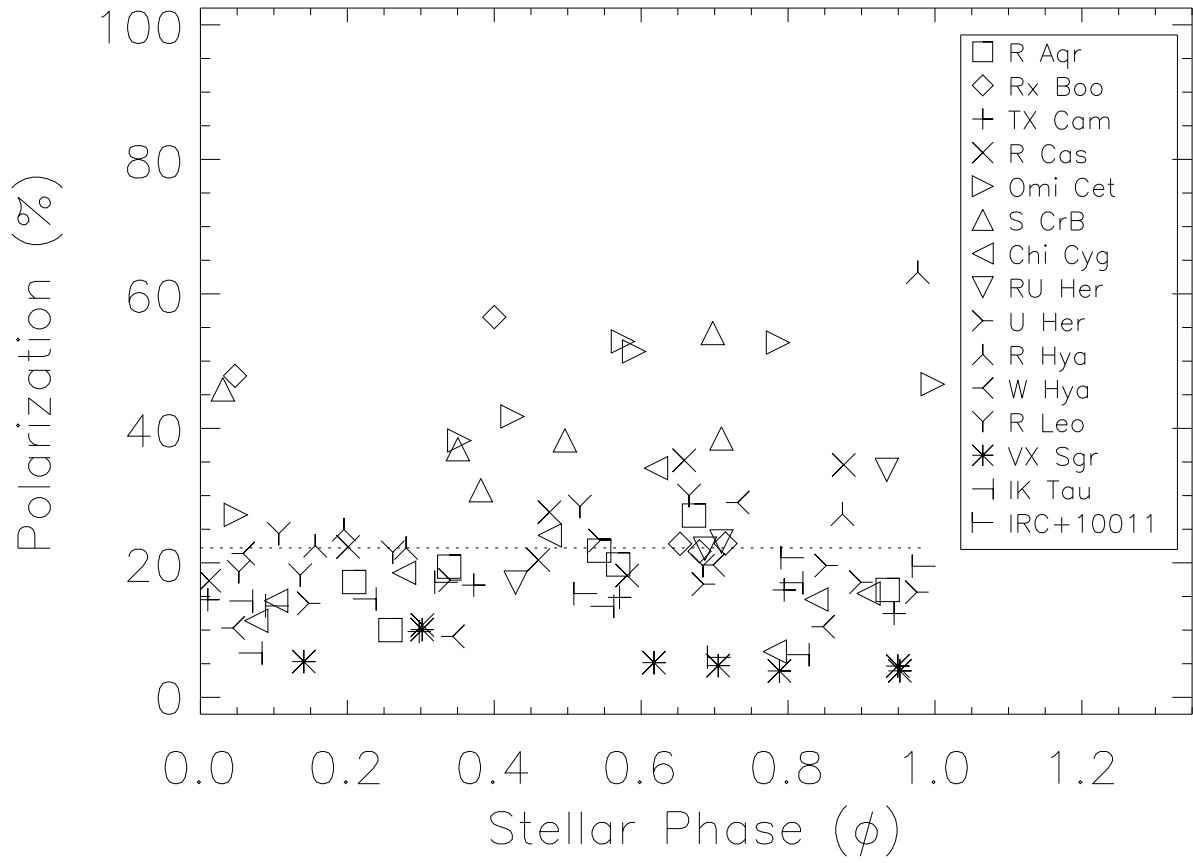


Fig. 4.— Line-integrated polarization as a function of stellar phase.

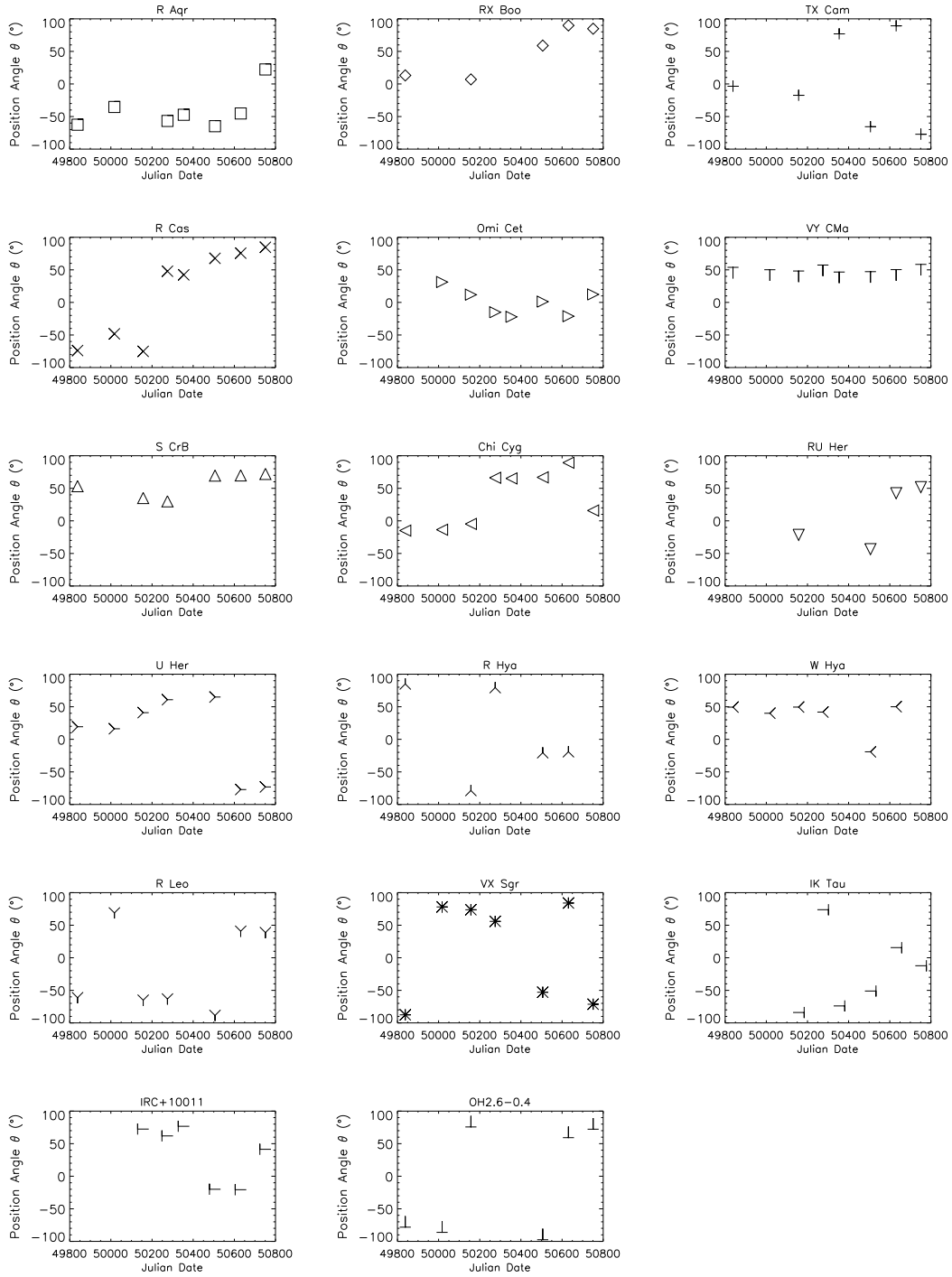


Fig. 5.— Line-integrated polarization position angle as a function of Julian Date. The full Julian Date for the first epoch of observations is 2449838.

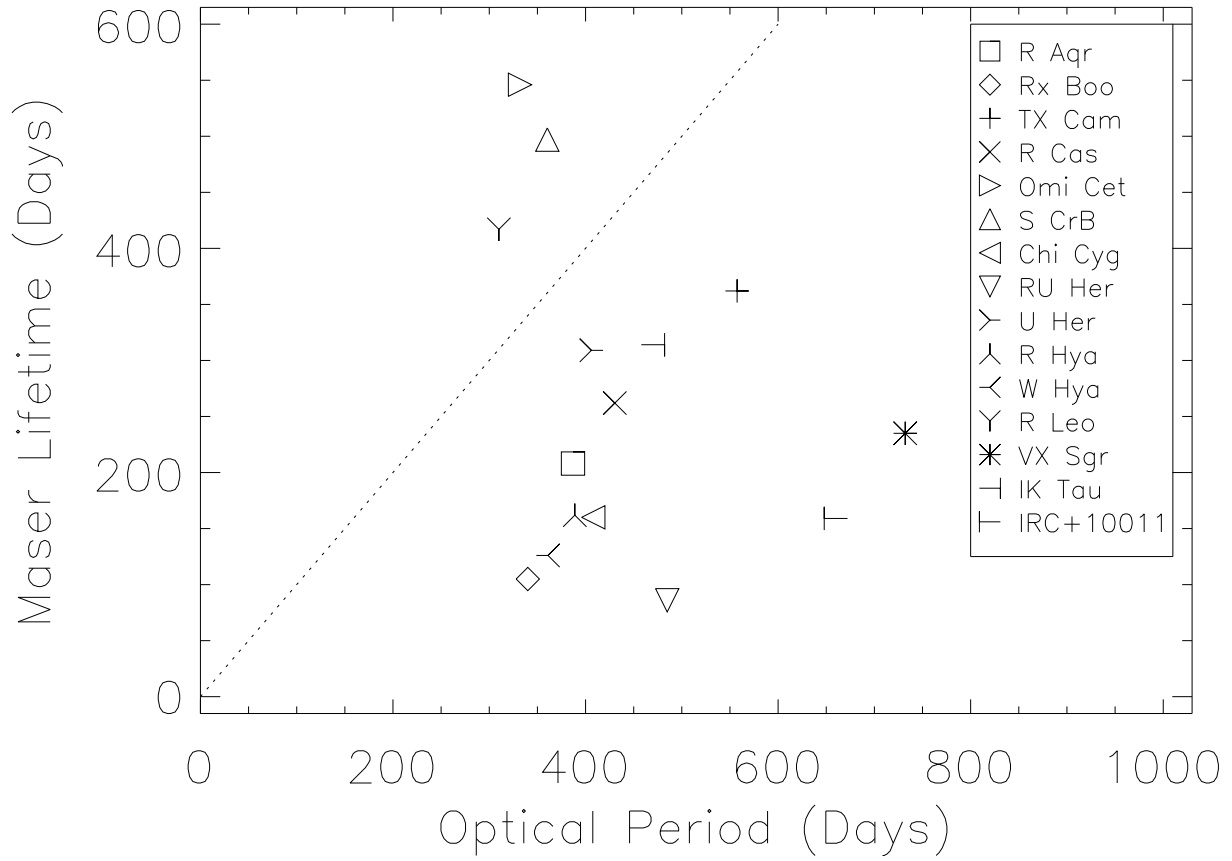


Fig. 6.— Characteristic maser spectral line feature lifetime versus optical period for all the periodic stars in the survey. The maser lifetimes were derived by correlating all the pairs of spectra at different epochs for each star. The dotted line has a slope of one; it is meant to show that most of the derived lifetimes are shorter than the stellar periods.

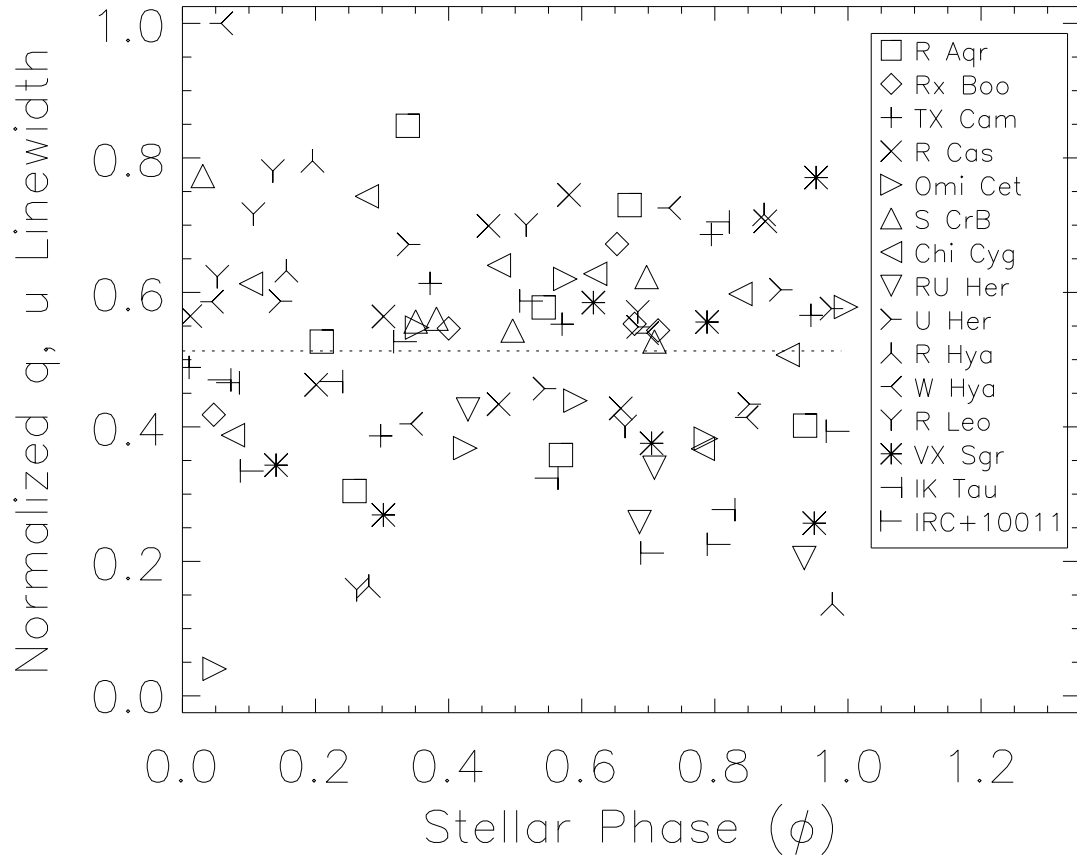


Fig. 7.— Maser polarization feature linewidths versus stellar phase. The linewidths were derived from the widths of the autocorrelation function of the q, u spectra for each epoch. For each star, the line width in km/s at each epoch was normalized by the maximum observed linewidth.

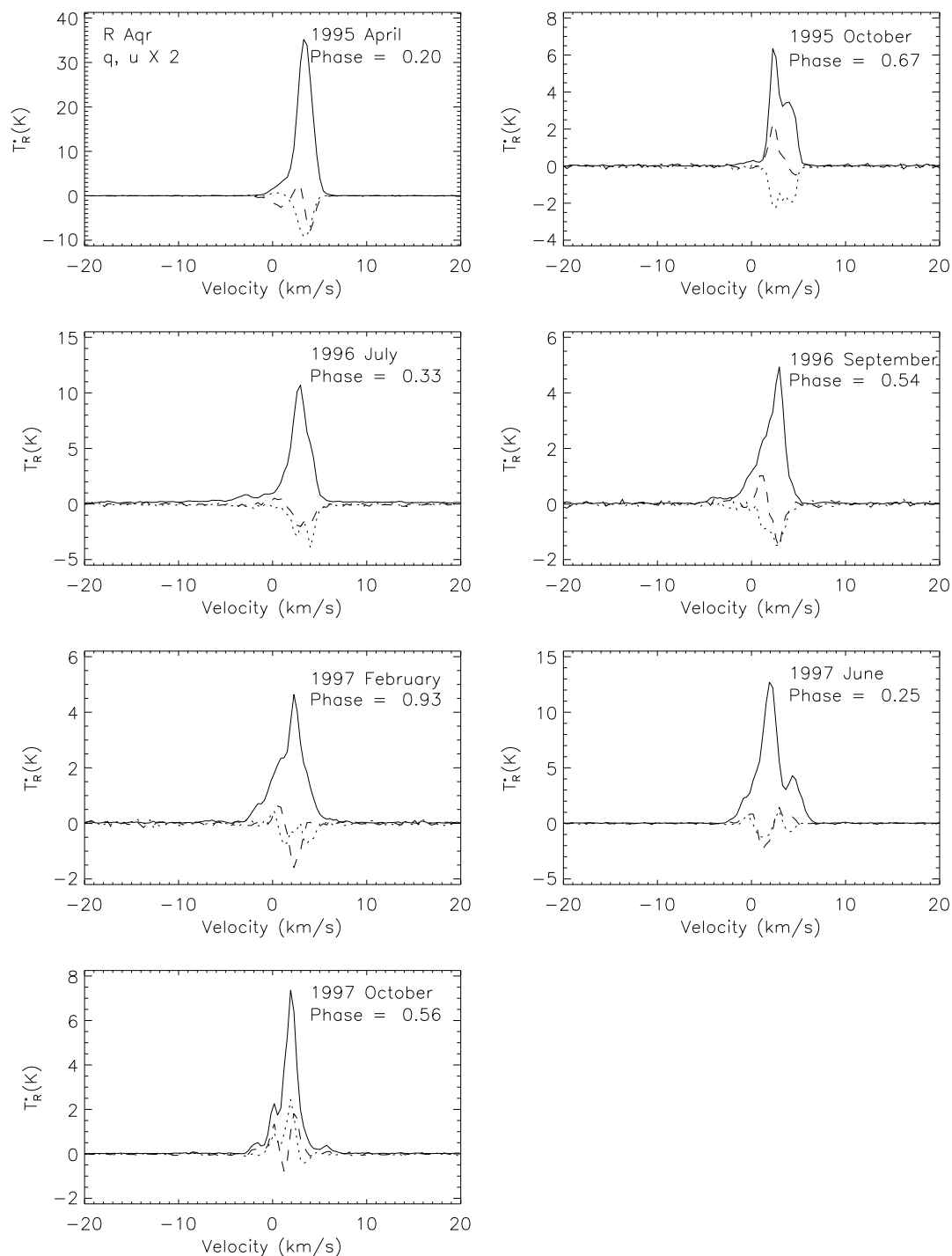


Fig. 8.— SiO line temperature and polarization spectra for R Aqr. There is one panel per epoch in which the star was observed. The phase for each epoch is given. The non-normalized Stokes parameters, q (dashed lines) and u (dotted lines), have been multiplied by two in all of the panels.

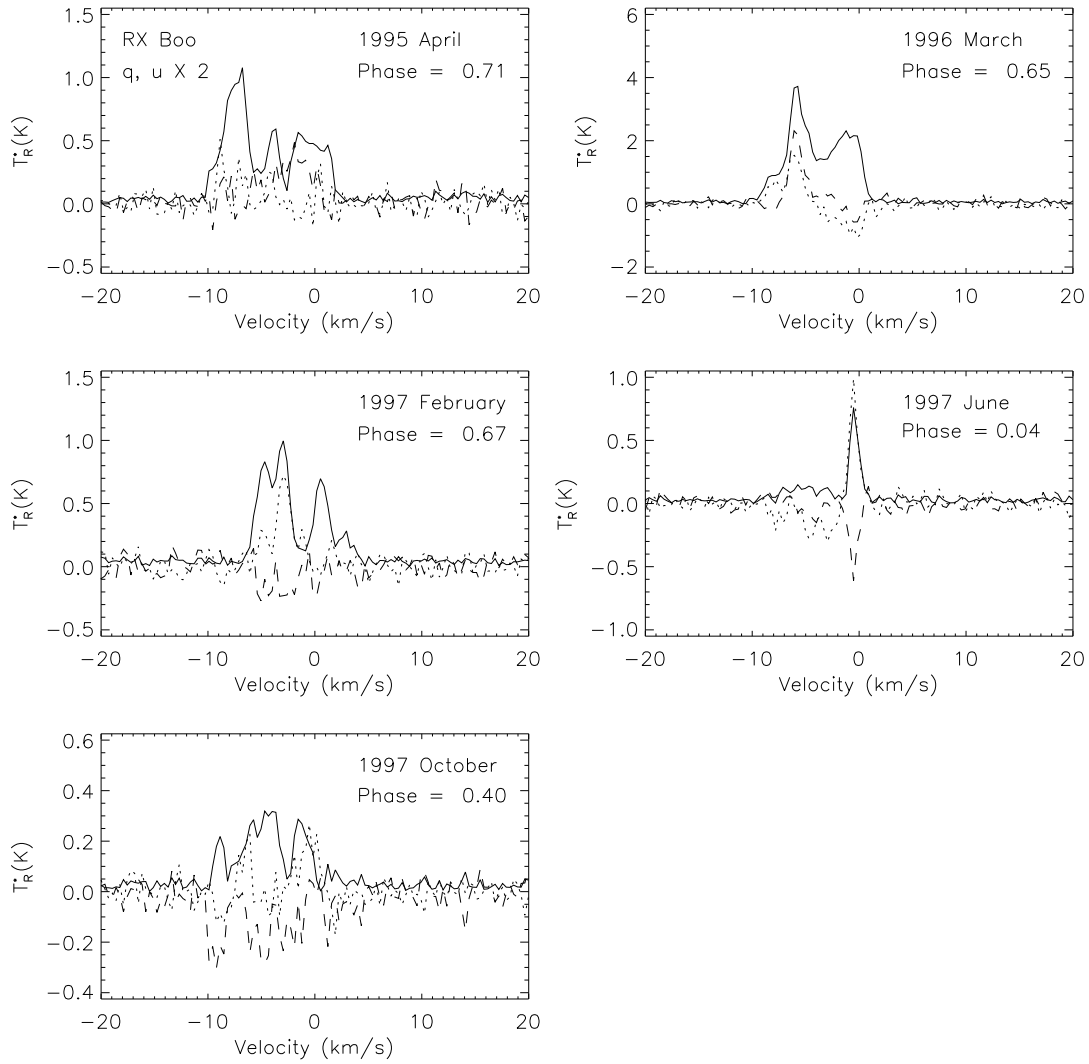


Fig. 9.— SiO line temperature and polarization spectra for RX Boo. The non-normalized Stokes parameters, q (dashed lines) and u (dotted lines), have been multiplied by two in all of the panels.

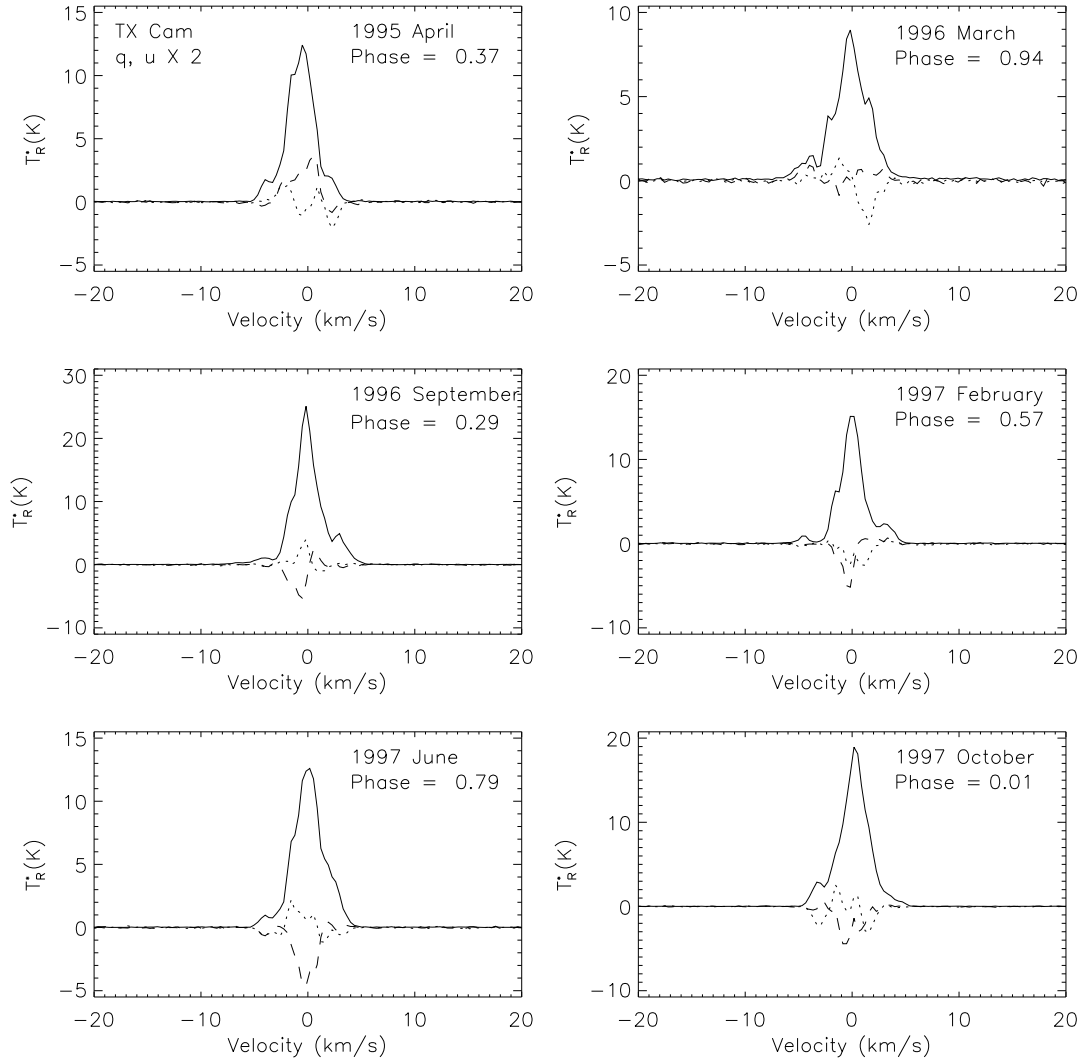


Fig. 10.— SiO line temperature and polarization spectra for TX Cam. The non-normalized Stokes parameters, q (dashed lines) and u (dotted lines), have been multiplied by two in all of the panels.

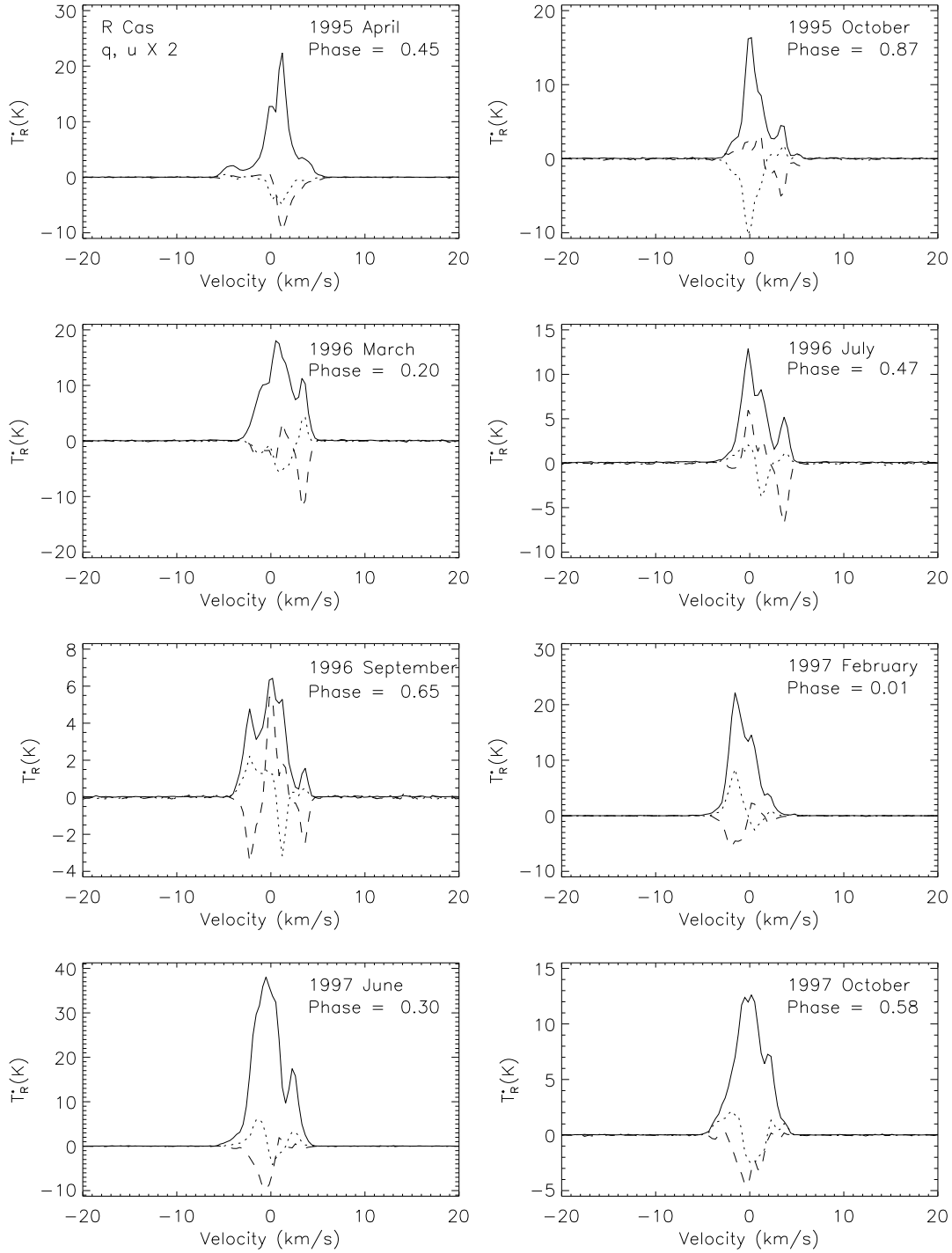


Fig. 11.— SiO line temperature and polarization spectra for R Cas. The non-normalized Stokes parameters, q (dashed lines) and u (dotted lines), have been multiplied by two in all of the panels.

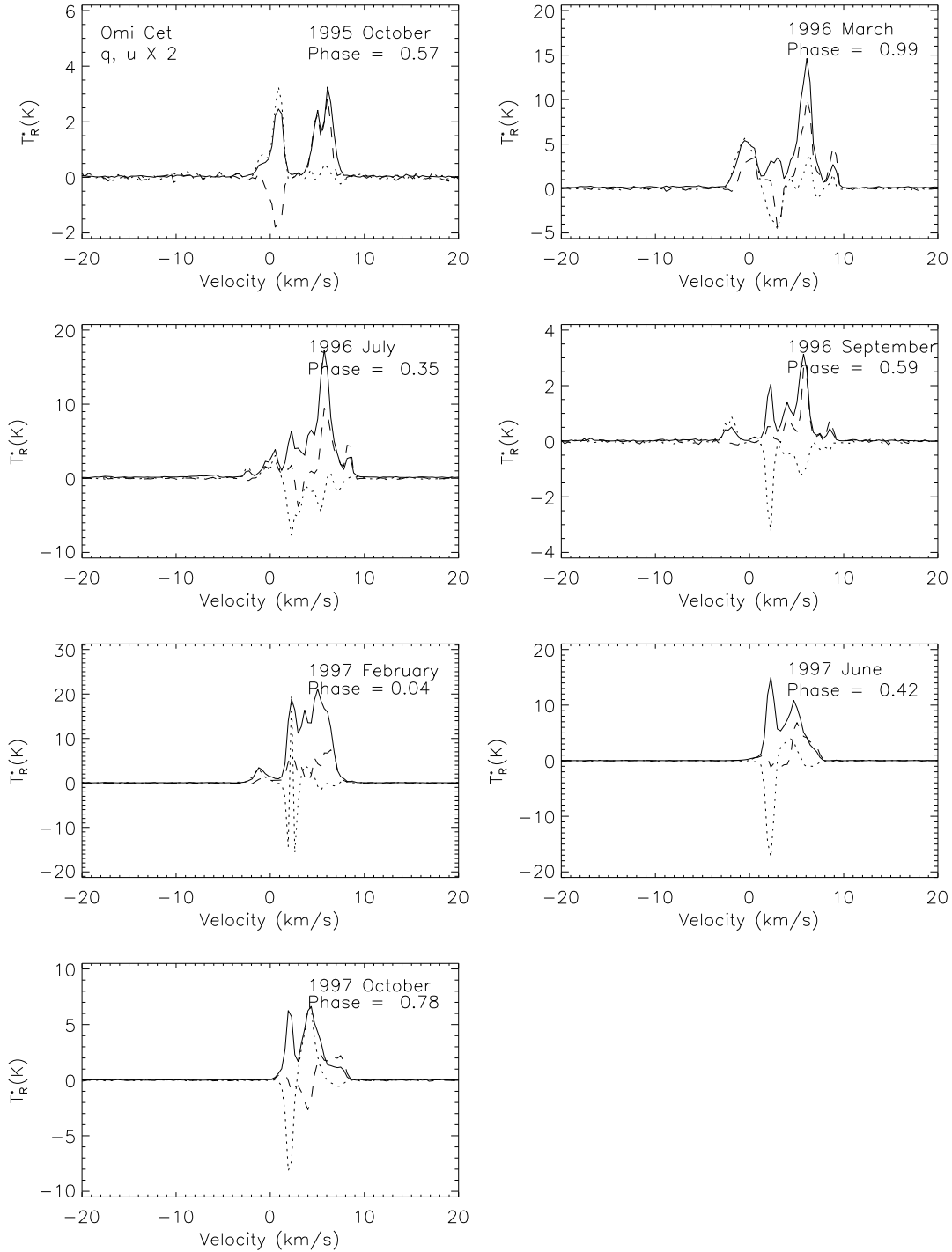


Fig. 12.— SiO line temperature and polarization spectra for Omi Ceti. The non-normalized Stokes parameters, q (dashed lines) and u (dotted lines), have been multiplied by two in all of the panels.

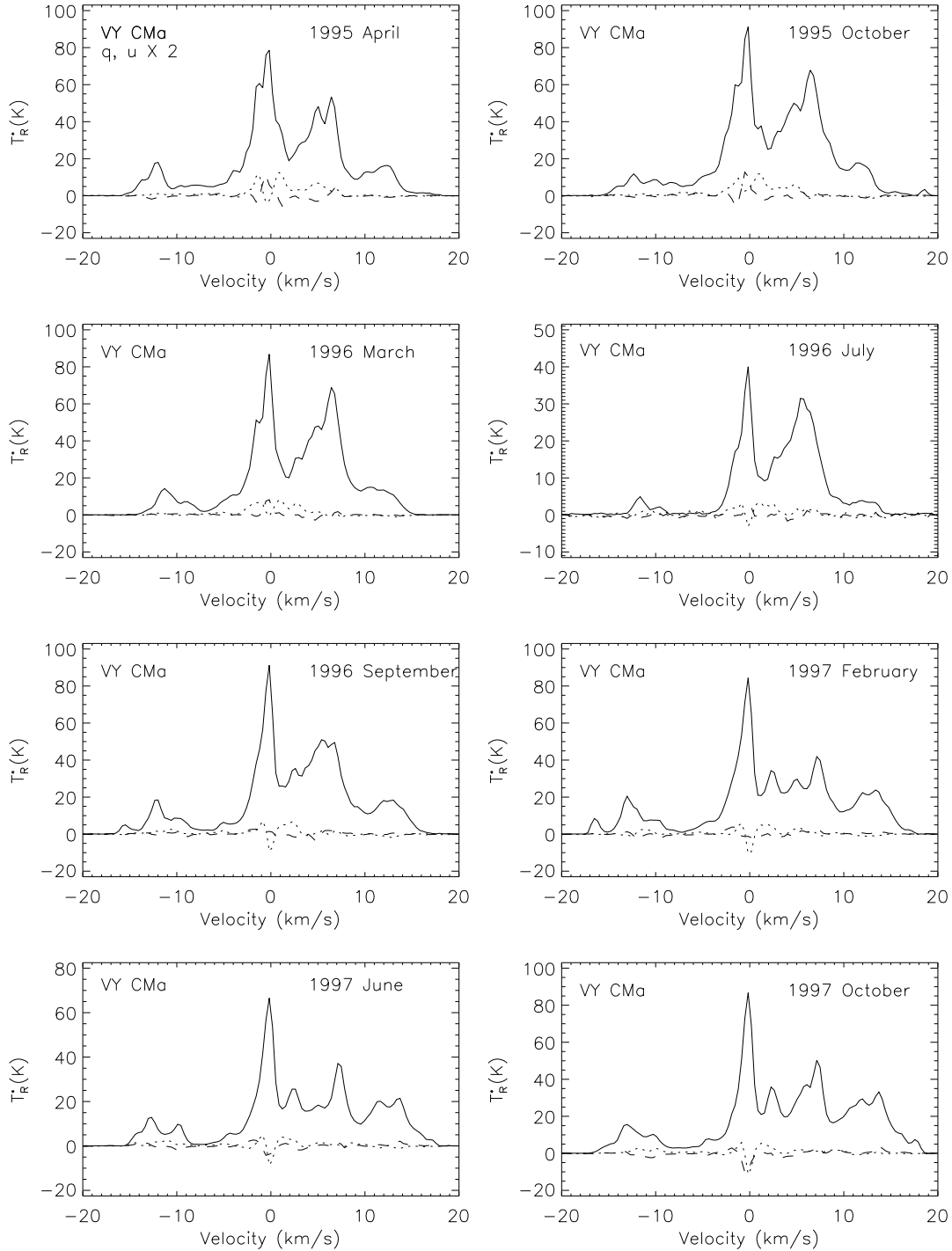


Fig. 13.— SiO line temperature and polarization spectra for VY CMa. The non-normalized Stokes parameters, q (dashed lines) and u (dotted lines), have been multiplied by two in all of the panels.

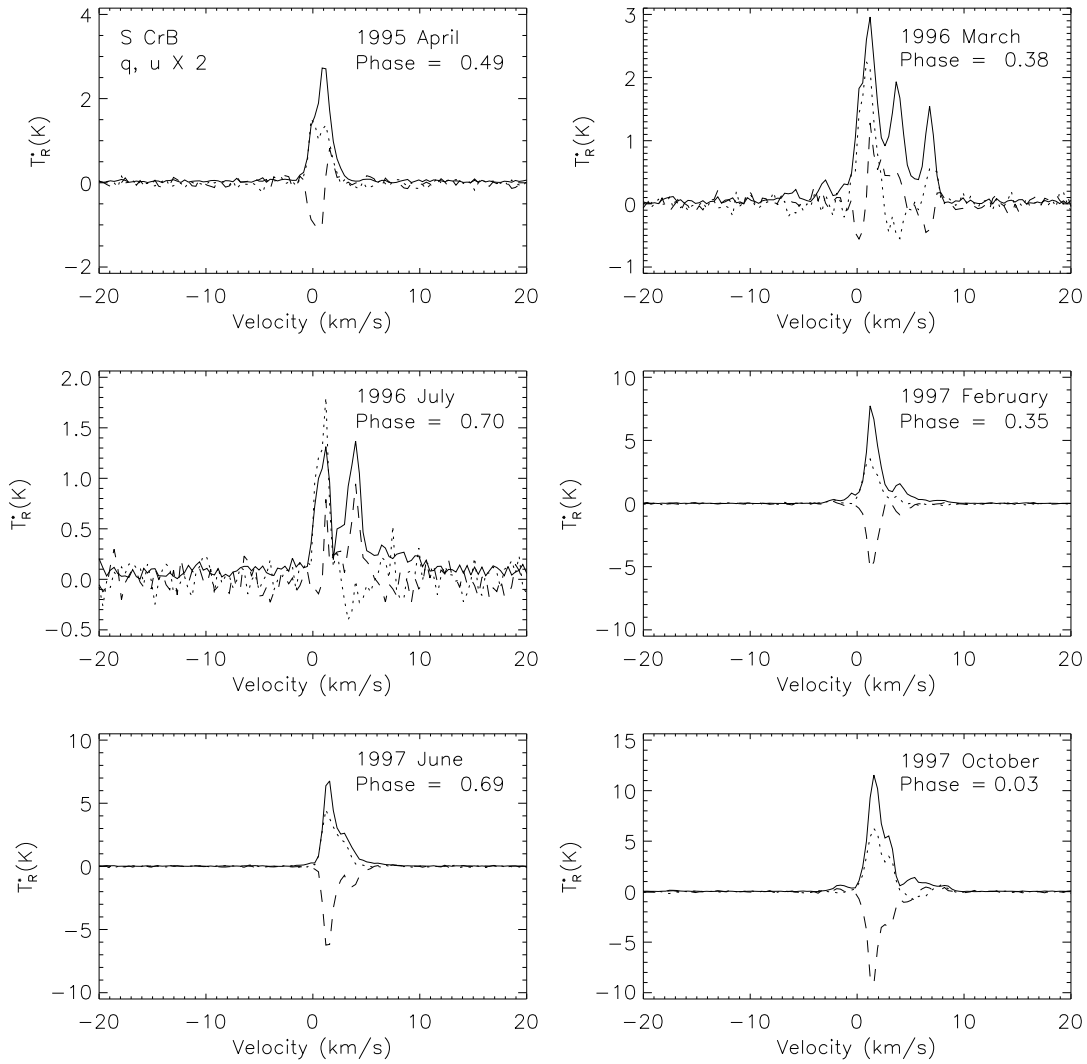


Fig. 14.— SiO line temperature and polarization spectra for S CrB. The non-normalized Stokes parameters, q (dashed lines) and u (dotted lines), have been multiplied by two in all of the panels.

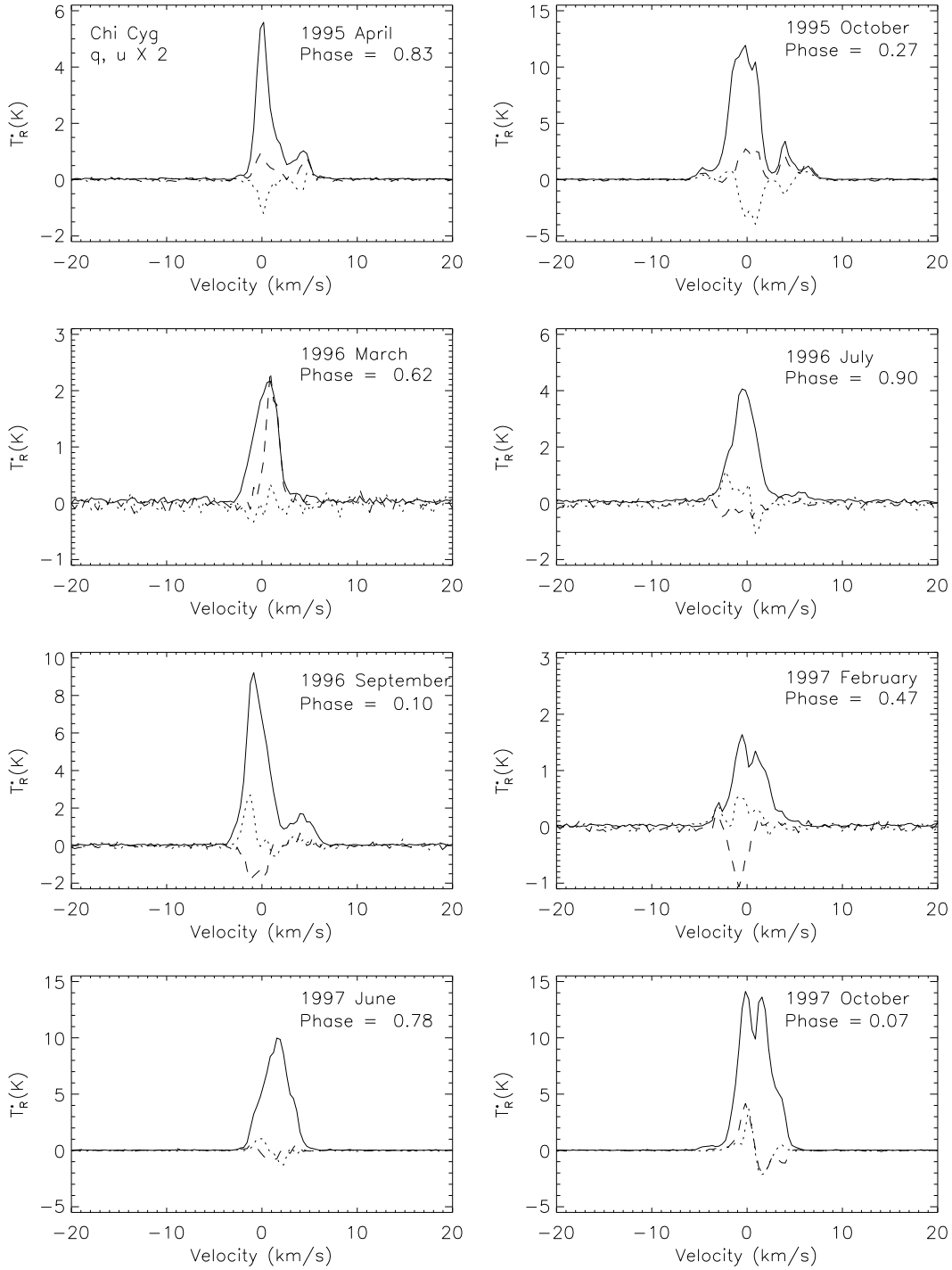


Fig. 15.— SiO line temperature and polarization spectra for Chi Cyg. The non-normalized Stokes parameters, q (dashed lines) and u (dotted lines), have been multiplied by two in all of the panels.

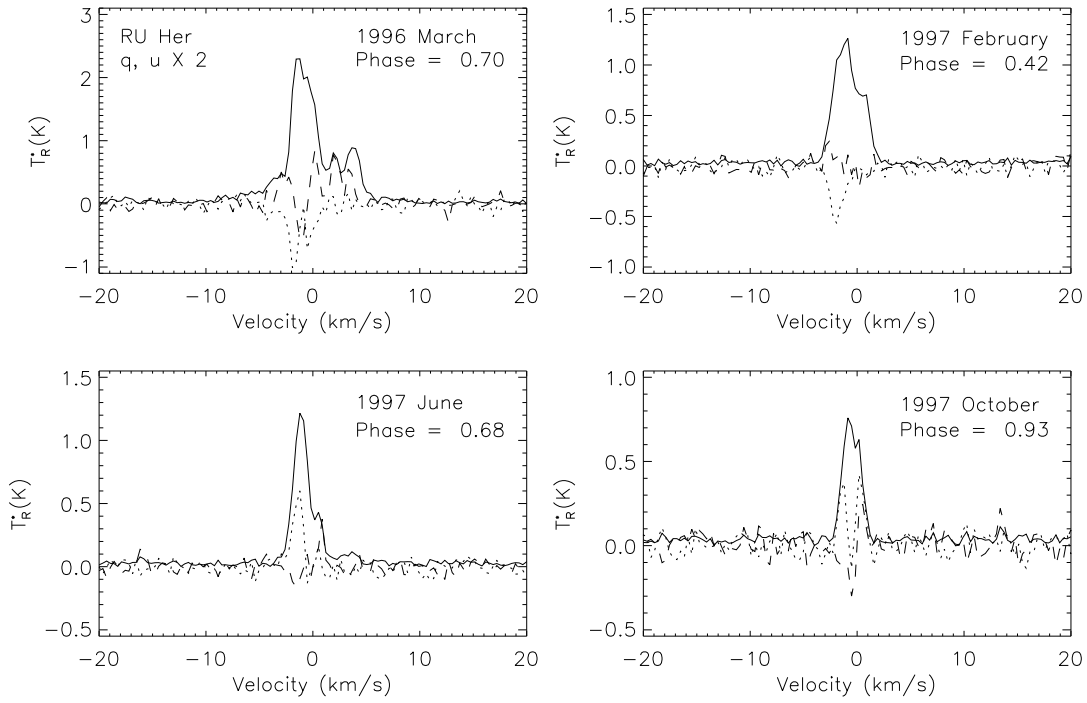


Fig. 16.— SiO line temperature and polarization spectra for RU Her. The non-normalized Stokes parameters, q (dashed lines) and u (dotted lines), have been multiplied by two in all of the panels.

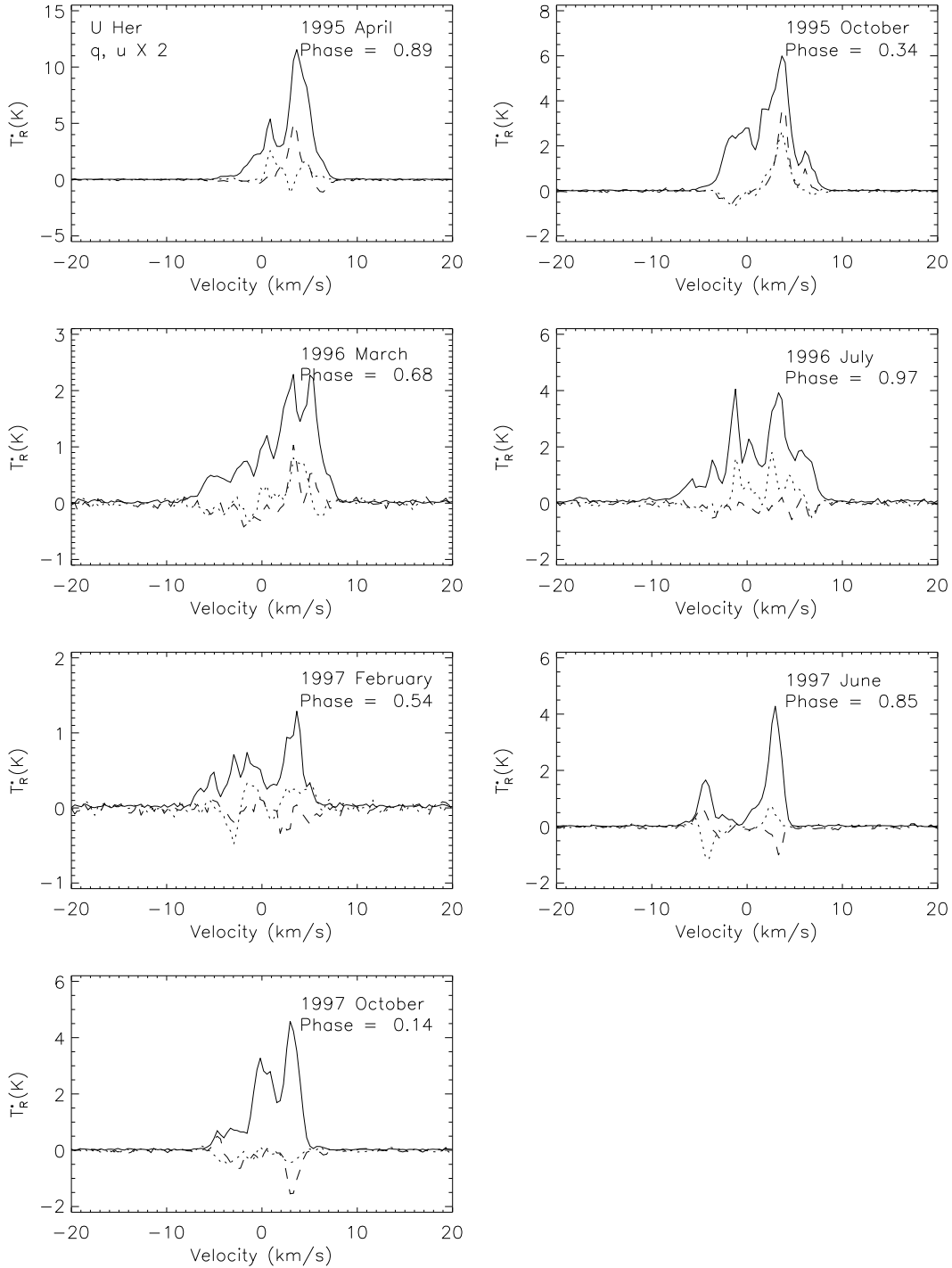


Fig. 17.— SiO line temperature and polarization spectra for U Her. The non-normalized Stokes parameters, q (dashed lines) and u (dotted lines), have been multiplied by two in all of the panels.

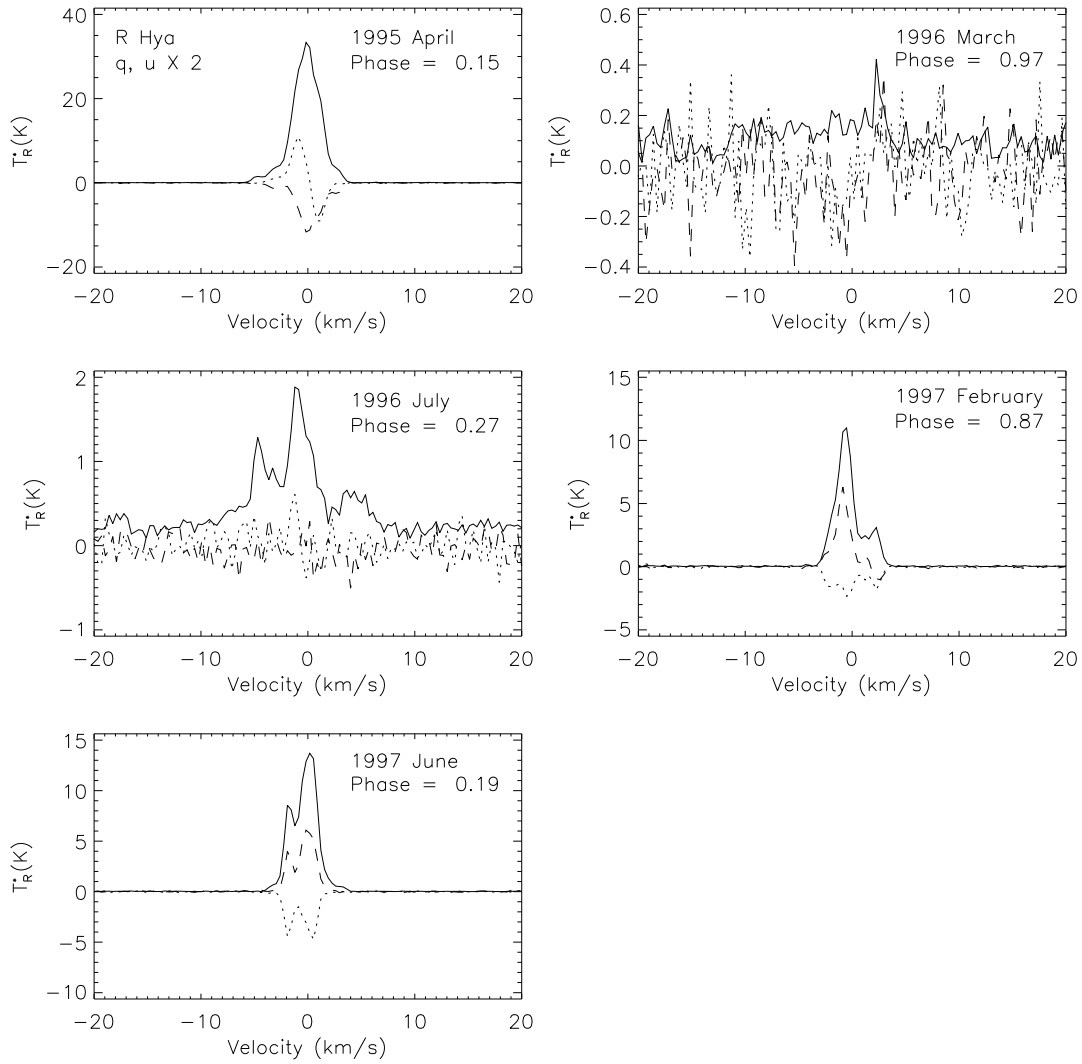


Fig. 18.— SiO line temperature and polarization spectra for R Hya. The non-normalized Stokes parameters, q (dashed lines) and u (dotted lines), have been multiplied by two in all of the panels.

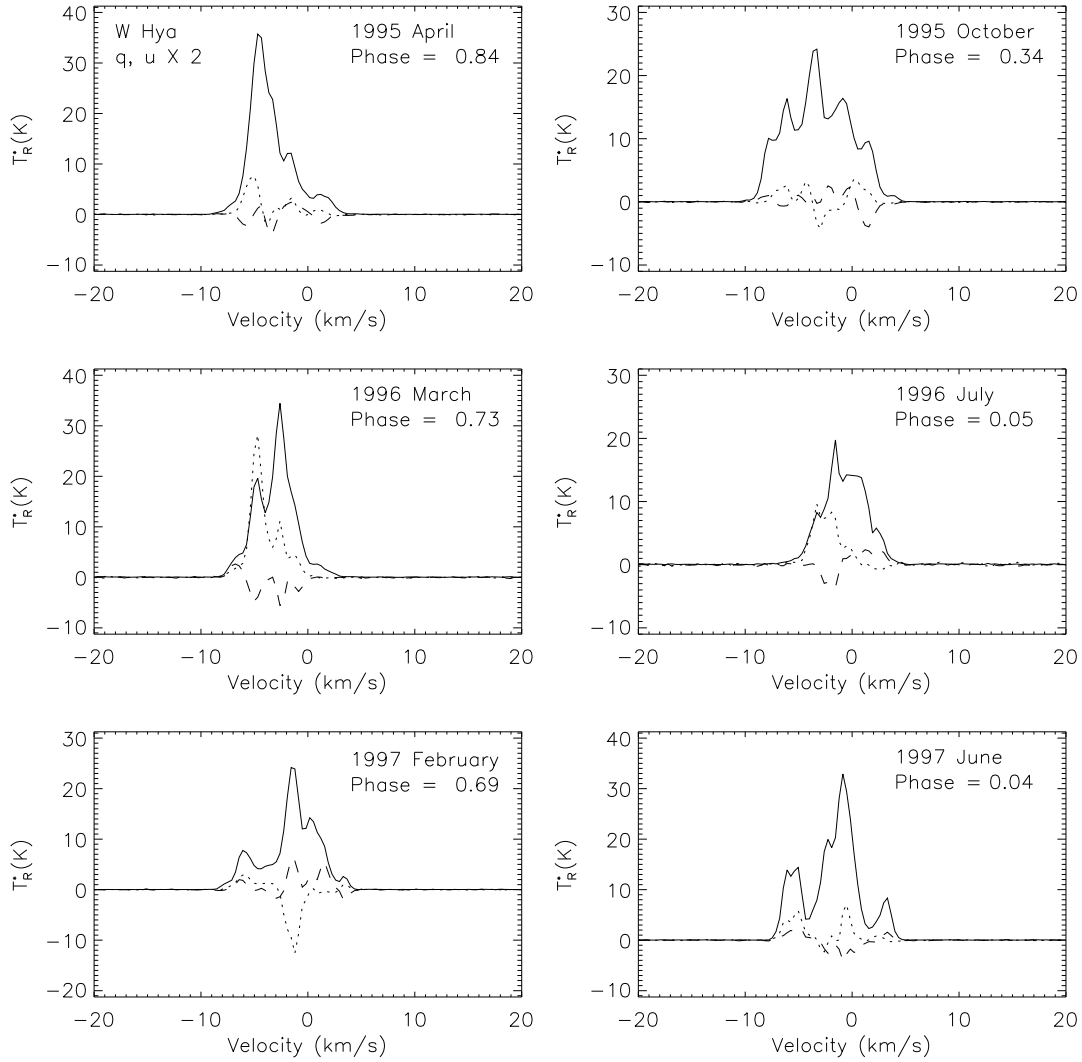


Fig. 19.— SiO line temperature and polarization spectra for W Hya. The non-normalized Stokes parameters, q (dashed lines) and u (dotted lines), have been multiplied by two in all of the panels.

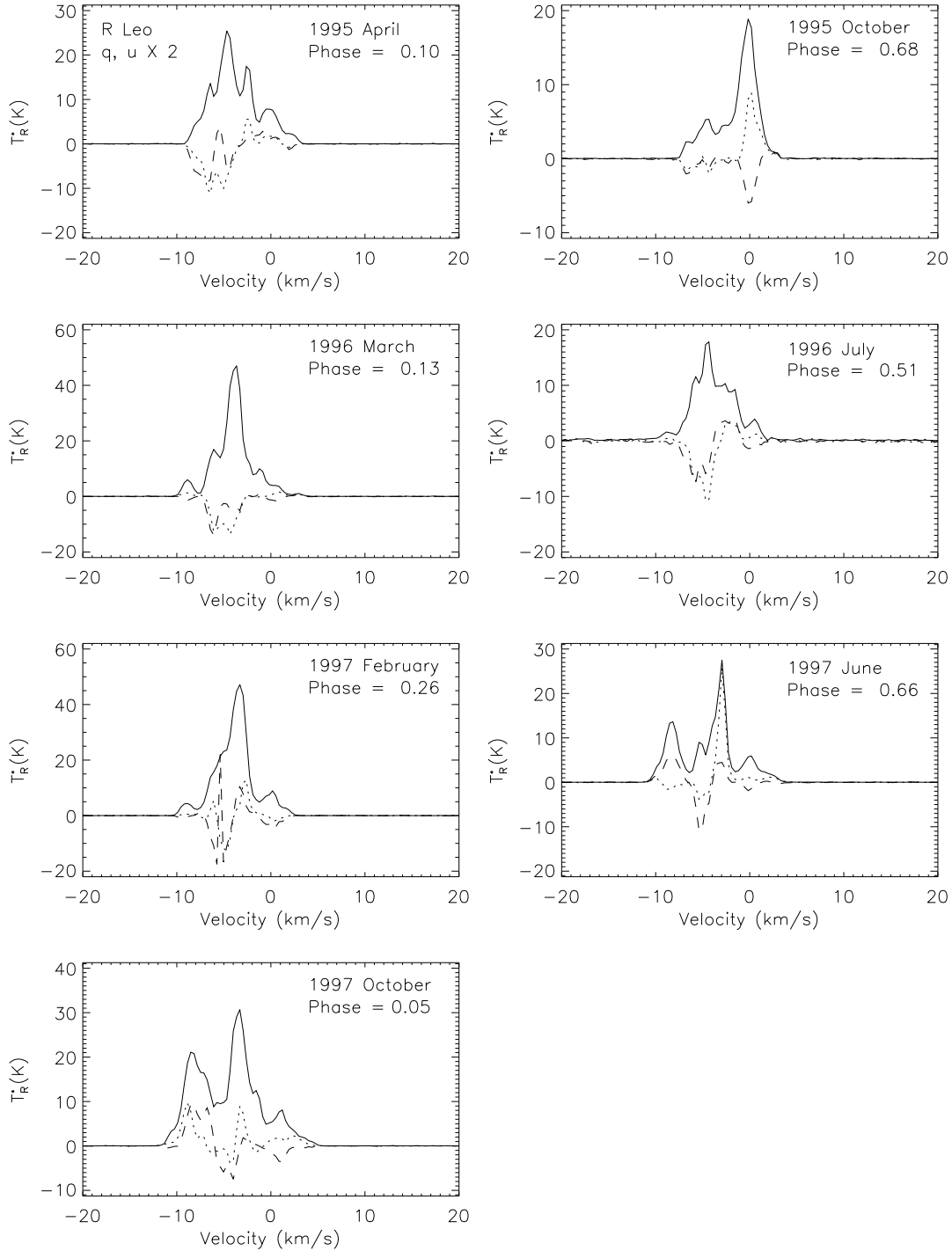


Fig. 20.— SiO line temperature and polarization spectra for R Leo. The non-normalized Stokes parameters, q (dashed lines) and u (dotted lines), have been multiplied by two in all of the panels.

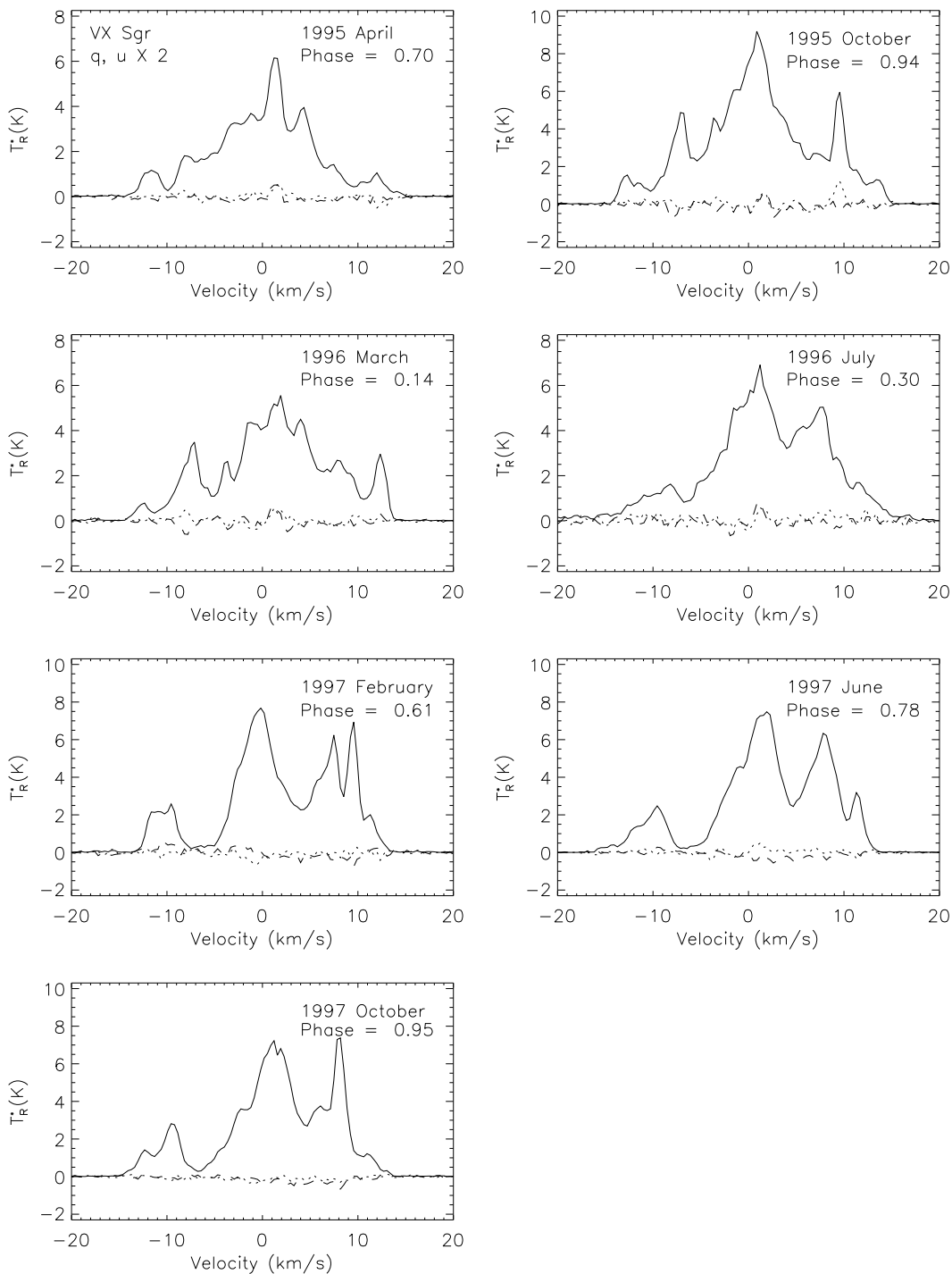


Fig. 21.— SiO line temperature and polarization spectra for VX Sgr. The non-normalized Stokes parameters, q (dashed lines) and u (dotted lines), have been multiplied by two in all of the panels.

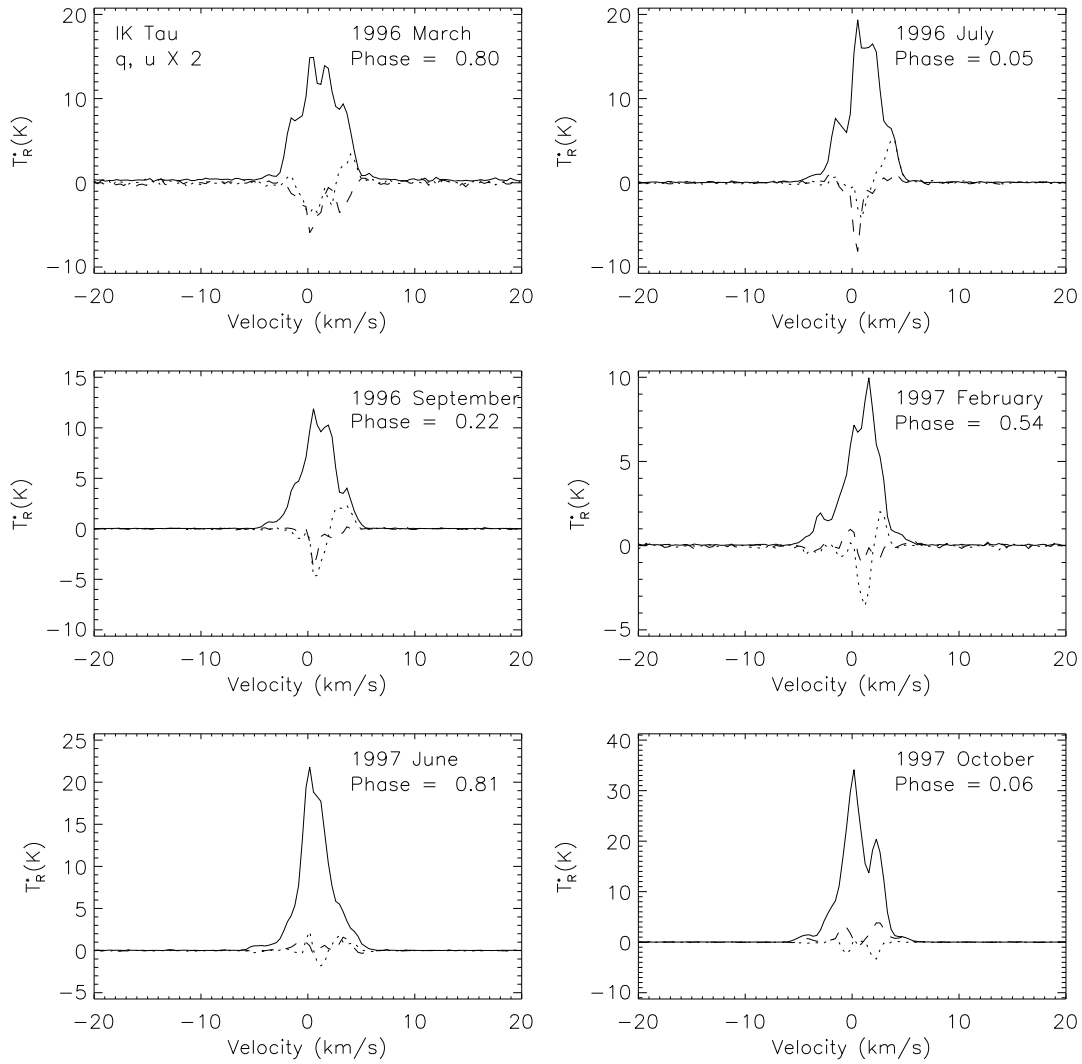


Fig. 22.— SiO line temperature and polarization spectra for IK Tau. The non-normalized Stokes parameters, q (dashed lines) and u (dotted lines), have been multiplied by two in all of the panels.

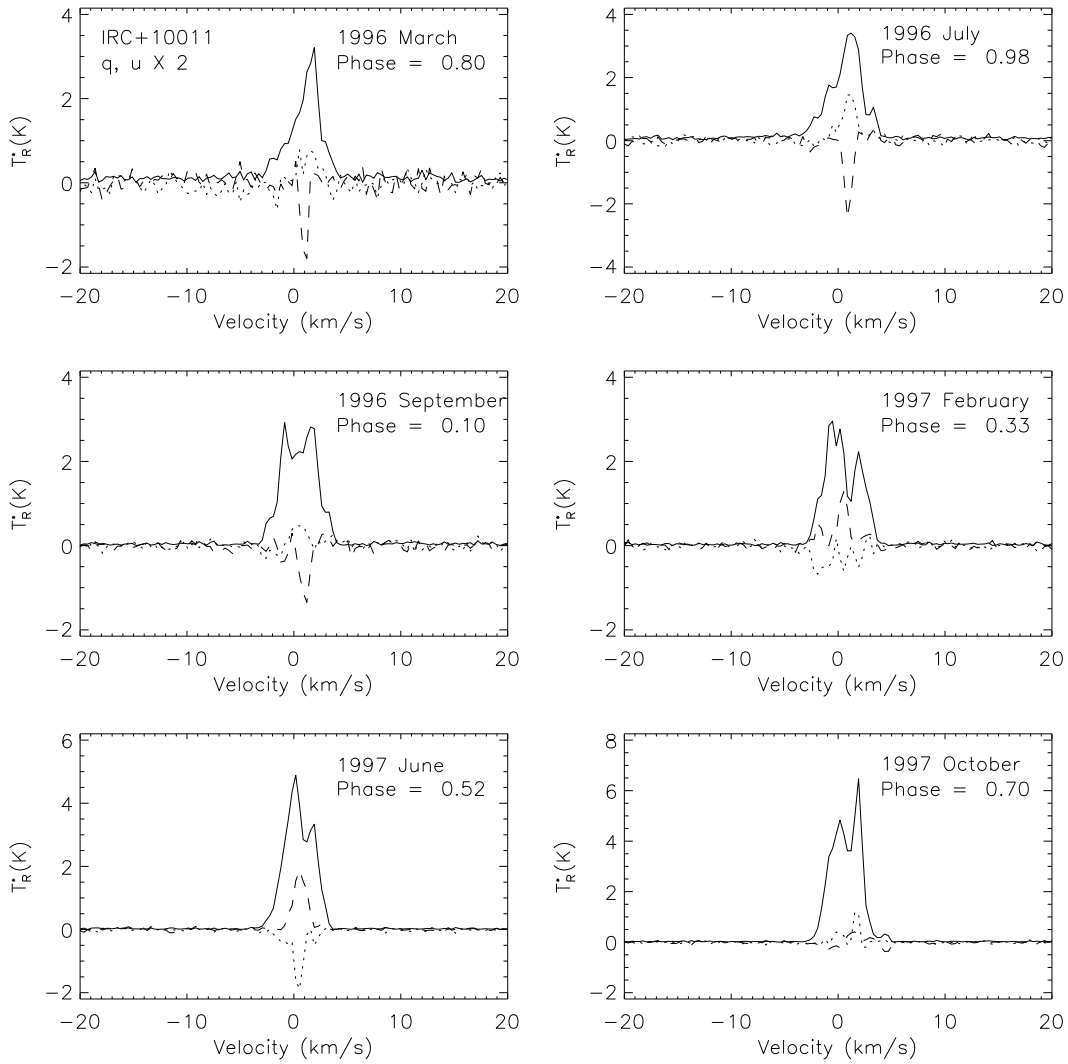


Fig. 23.— SiO line temperature and polarization spectra for IRC+10011. The non-normalized Stokes parameters, q (dashed lines) and u (dotted lines), have been multiplied by two in all of the panels.

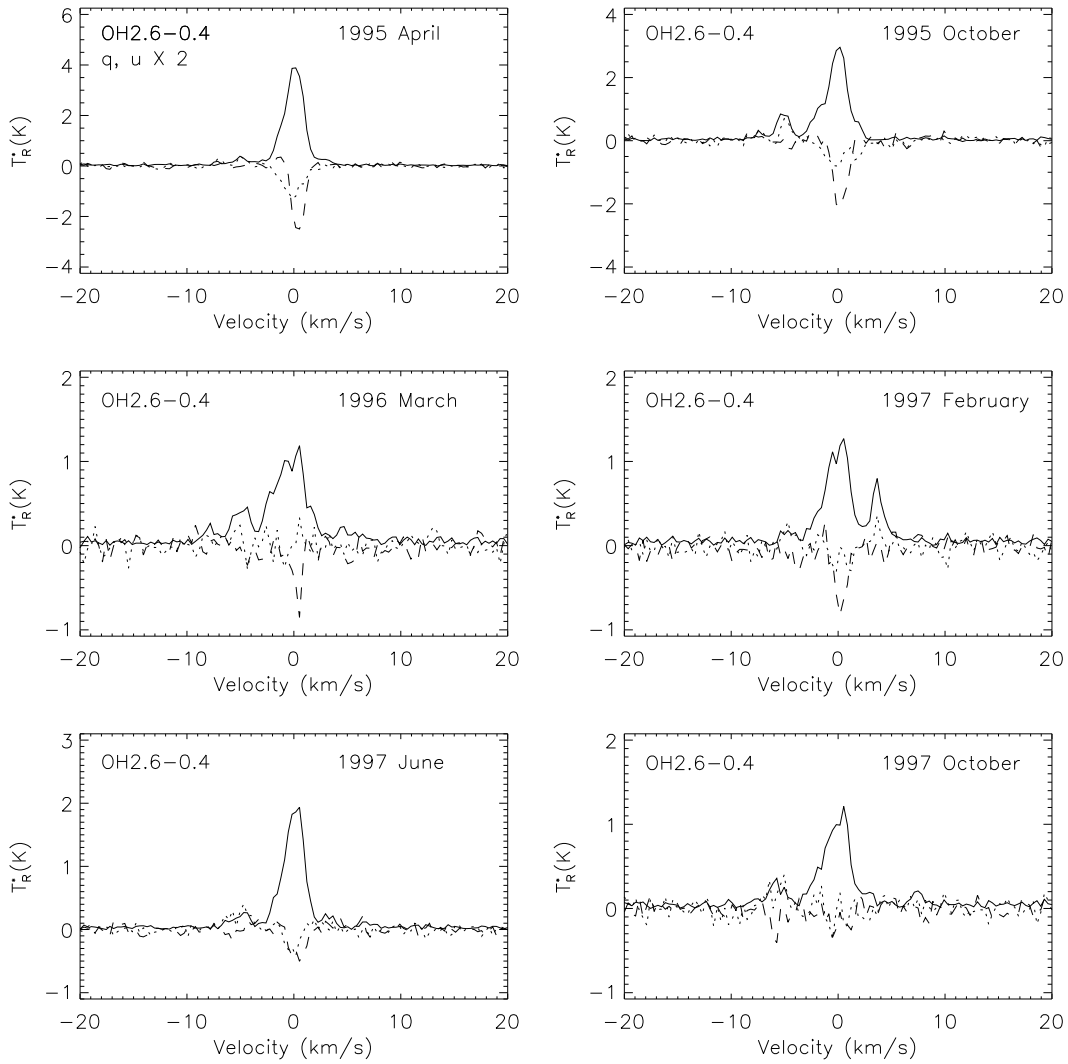


Fig. 24.— SiO line temperature and polarization spectra for OH2.6-0.4. The non-normalized Stokes parameters, q (dashed lines) and u (dotted lines), have been multiplied by two in all of the panels.